

Muon $g - 2$ and semileptonic B decays in BDW model with gauge kinetic mixing

Sang Quang Dinh^a, and Hieu Minh Tran^{b,1}

^a*VNU University of Science, Vietnam National University - Hanoi,
334 Nguyen Trai Road, Hanoi, Vietnam*

^b*Hanoi University of Science and Technology, 1 Dai Co Viet Road, Hanoi, Vietnam*

Abstract

In the model proposed by Bélanger, Delaunay and Westhoff (BDW), a new sector consisted of vector-like fermions and two complex scalars is charged under an extra Abelian symmetry $U(1)_X$. In this paper, we generalize the BDW model by introducing the kinetic mixing between the $U(1)_X$ and the standard model $U(1)_Y$ gauge fields. The new physics contributions to the muon anomalous magnetic moment and the Wilson coefficients $C_{9,10}^{(\prime)}$ are obtained analytically. We have explored the free parameter space of the model, taking into account the constraints on the muon $g - 2$, the lepton universality violation in terms of R_K and R_{K^*} , and the branching ratios of the semileptonic decays, $B^+ \rightarrow K^+ \mu^+ \mu^-$ and $B^0 \rightarrow K^{*0} \mu^+ \mu^-$, as well as the perturbative requirement. The viable parameter regions of the model are identified. In the presence of the gauge kinetic mixing term, those regions are enlarged and significantly deformed in comparison to the case with vanishing kinetic mixing. In the near future, the E989 experiment will be able to test significant parts of the currently allowed parameter regions.

¹E-mail: hieu.tranminh@hust.edu.vn

1 Introduction

Although the standard model (SM) predictions have been verified in many experiments showing an excellent agreement with data, new physics seems to be around the corner due to unanswered questions. On the one hand, one of the most important precision tests of the SM is the muon anomalous magnetic moment ($g - 2$) whose value was determined accurately as [1]

$$a_\mu^{\text{exp}} = (11659209.1 \pm 6.3) \times 10^{-10}. \quad (1)$$

However, the SM prediction for the muon $g - 2$ is presently [2]

$$a_\mu^{\text{SM}} = (11659181.0 \pm 4.3) \times 10^{-10}, \quad (2)$$

corresponding to a 3.7σ deviation from the above world-average experimental value. In the currently running experiment (E989) at Fermilab [3] as well as the future experiment (E34) at J-PARC [4], the precision will be improved by a factor of four that will shed light on this deviation. If the experimental center value of the muon $g - 2$ remains unchanged, the above deviation will raise up to about $6-7\sigma$ [5], evidently indicating the existence of new physics coupled to the lepton sector [6].

On the other hand, with the improvement of experimental accuracy, rare decays of B -mesons are useful as the precision tests of the SM. The small branching ratios of these processes make them good probes to search for new physics beyond the SM. In fact, anomalies have been observed in the rare semileptonic B decays related to the quark transition process $b \rightarrow s\ell^+\ell^-$. In particular, the measured relative branching ratios for $1.1 \text{ GeV} < q^2 < 6.0 \text{ GeV}$ [7, 8]

$$R_K = \frac{BR(B^+ \rightarrow K^+\mu^+\mu^-)}{BR(B^+ \rightarrow K^+e^+e^-)} = 0.846_{-0.056}^{+0.062}, \quad (3)$$

$$R_{K^*} = \frac{BR(B^0 \rightarrow K^{*0}\mu^+\mu^-)}{BR(B^0 \rightarrow K^{*0}e^+e^-)} = 0.71_{-0.09}^{+0.12}, \quad (4)$$

deviate from the corresponding SM predictions being close to unity [9, 10, 11] at the levels of 2.5σ and 2.4σ , respectively [12, 13]. This may be a signature of the lepton universality violation implying the existence of new physics beyond the SM. Recently, the updated LHCb results on the angular analysis of the decay process $B^0 \rightarrow K^{*0}\mu^+\mu^-$ show a 3.3σ deviation from the SM prediction [14, 15] that is slightly increased in comparison to the previous observation [16]. This is due to the higher statistics regarding to the inclusion of 2016 data for 13 TeV collisions.

Model independent analyses on the experimental data using the effective field theory approach with the Hamiltonian [17]

$$\mathcal{H}_{\text{eff}} = -\frac{\alpha G_F}{\sqrt{2}\pi} V_{tb} V_{ts}^* \sum_i (C_i \mathcal{O}_i + C'_i \mathcal{O}'_i) + h.c., \quad (5)$$

where α and G_F are the fine structure constant and the Fermi constant, have been performed to determine the new physics contributions to the relevant Wilson coefficients [18]

$$C_i^{(\prime)} = C_i^{(\prime)\text{SM}} + C_i^{(\prime)\text{NP}}, \quad (6)$$

corresponding to the operators

$$\mathcal{O}_7^{(\prime)} = \frac{m_b}{e} [\bar{s}\sigma_{\mu\nu}P_{R(L)}b] F^{\mu\nu}, \quad (7)$$

$$\mathcal{O}_9^{(\prime)} = [\bar{s}\gamma_\mu P_{L(R)}b] [\bar{\ell}\gamma^\mu\ell], \quad (8)$$

$$\mathcal{O}_{10}^{(\prime)} = [\bar{s}\gamma_\mu P_{L(R)}b] [\bar{\ell}\gamma^\mu\gamma_5\ell], \quad (9)$$

$$\mathcal{O}_S^{(\prime)} = [\bar{s}P_{R(L)}b] [\bar{\ell}\ell], \quad (10)$$

$$\mathcal{O}_P^{(\prime)} = [\bar{s}P_{R(L)}b] [\bar{\ell}\gamma_5\ell]. \quad (11)$$

The Wilson coefficients $C_{S,P}^{(\prime)}$ and $C_7^{(\prime)}$ are strictly constrained by the leptonic decay process $B_s \rightarrow \mu^+\mu^-$ [19] and the radiative B decays [20], respectively. In the case of semileptonic decays of B mesons, the fitting results showed that scenarios with new physics contributions to the Wilson coefficients is much more favored than the pure SM, especially for the coefficient C_9^μ . While the new physics contributions to muonic Wilson coefficients ($C_9^{\mu(\prime)}, C_{10}^{\mu(\prime)}$) play an important role, the electronic coefficients ($C_9^{e(\prime)}, C_{10}^{e(\prime)}$) turn out to be consistent with the SM predictions. Three preferable 1D scenarios for the new physics contribution to muonic coefficients have been found to be: (i) C_9^{NP} only, (ii) $C_9^{\text{NP}} = -C_{10}^{\text{NP}}$, and (iii) $C_9^{\text{NP}} = -C_{10}^{\text{NP}}$ respectively [21]. However, the third scenario is disfavored since it predicts $R_{K^*} \approx 1$ [22]. The 2D scenarios were also investigated [13]. The fitting to the experimental data with complex Wilson coefficients was performed in Ref. [23].

Many models have been invented to address the anomalies in the semileptonic decays of B mesons, for example those including a Z' boson resulting from an extended gauge symmetry [24, 25, 26], leptoquarks [27], new physics contributions via loop corrections [28], or supersymmetry [29]. In this paper, we investigate the model proposed by Bélanger, Delaunay and Westhoff (BDW) in Ref. [30] taking into account the gauge kinetic mixing. In this model, new particles introduced beyond the SM ones are vector-like quarks and leptons, and two complex scalars. The model's gauge symmetry is $SU(3)_C \times SU(2)_L \times U(1)_Y \times U(1)_X$ where the additional Abelian symmetry is broken spontaneously resulting in a massive gauge boson Z' . In the presence of the gauge kinetic mixing, we calculate analytically the new physics contributions to the muon $g-2$, and the Wilson coefficients $C_{9,10}^{(\prime)}$ which are used to compute the B -meson semileptonic decays. The most updated data from the Heavy Flavor Averaging Group [31] and the LHCb Collaboration [7, 8] are used in our consideration to constrain the model's relevant parameters.

Using the projected sensitivity of the muon $g - 2$ experiment E989, we study its ability to test the model in the near future.

The structure of the paper is as follows. In Section 2, we briefly review the structure of the BDW model, then generalize it by introducing the gauge kinetic mixing. In Section 3, the analytic results of the new physics contributions to the muon $g - 2$ and the Wilson coefficients calculations are presented. In Section 4, the phenomenological constraints are used to specify the allowed parameter space. Finally, Section 5 is devoted to conclusions.

2 BDW model with kinetic mixing

2.1 The model

The new particles introduced in the BDW model beside the SM particles are the vector-like lepton and quark doublets of the gauge group $SU(2)_L$,

$$L_{L,R} = \begin{pmatrix} N_{L,R} \\ E_{L,R} \end{pmatrix}, \quad Q_{L,R} = \begin{pmatrix} U_{L,R} \\ D_{L,R} \end{pmatrix}, \quad (12)$$

and two complex scalars, χ and ϕ , that are singlets under the SM gauge groups. The symmetry of this model is an extension of the SM symmetry by adding an extra Abelian gauge group, namely $SU(3)_C \otimes SU(2)_L \otimes U(1)_Y \otimes U(1)_X$. The SM particles are invariant under $U(1)_X$ transformation, while the new particles transform nontrivially with the $U(1)_X$ charges given in Table 1 together with other properties.

Table 1: Properties of new particles introduced in the model [30].

Particles	Spin	$SU(3)_C$	$SU(2)_L$	$U(1)_Y$	$U(1)_X$
L_L, L_R	1/2	1	2	-1/2	1
Q_L, Q_R	1/2	3	2	1/6	-2
χ	0	1	1	0	-1
ϕ	0	1	1	0	2

The Lagrangian include the SM part and the part involving new physics:

$$\mathcal{L} = \mathcal{L}_{\text{SM}} + \mathcal{L}_{\text{NP}}, \quad (13)$$

where

$$\begin{aligned} \mathcal{L}_{\text{NP}} \supset & -\lambda_{\phi H} |\phi|^2 |H|^2 - \lambda_{\chi H} |\chi|^2 |H|^2 - [y \bar{\ell}_L L_R \chi + w \bar{q}_L Q_R \phi + h.c.] - V_0(\phi, \chi) \\ & - (M_L \bar{L}_L L_R + M_Q \bar{Q}_L Q_R + h.c.), \end{aligned} \quad (14)$$

Here, the SM left-handed lepton and quark doublets are denoted as

$$\ell_L^i = \begin{pmatrix} \nu_L^e \\ e_L \end{pmatrix}_i, \quad q_L^i = \begin{pmatrix} u_L \\ d_L \end{pmatrix}_i, \quad (i = 1, 2, 3). \quad (15)$$

The explicit form of the scalar potential $V_0(\chi, \phi)$ is given by

$$V_0(\chi, \phi) = \lambda_\phi |\phi|^4 + m_\phi^2 |\phi|^2 + \lambda_\chi |\chi|^4 + m_\chi^2 |\chi|^2 + \lambda_{\phi\chi} |\phi|^2 |\chi|^2 + (r\phi\chi^2 + h.c.). \quad (16)$$

Among the new scalars, we assume that only ϕ can develop a vacuum expectation value (VEV),

$$\langle \phi \rangle = \sqrt{\frac{-m_\phi'^2}{2\lambda_\phi}}, \quad (17)$$

where

$$m_\phi'^2 = m_\phi^2 + \lambda_{\phi H} \langle H \rangle^2, \quad (18)$$

with $\langle H \rangle = 174$ GeV being the VEV of the SM Higgs field. Due to the nonzero VEV, $\langle \phi \rangle$, the gauge group $U(1)_X$ is spontaneously broken, leading to a massive Z' boson with a mass

$$m_{Z'} = 2\sqrt{2}g_X \langle \phi \rangle. \quad (19)$$

where g_X is the $U(1)_X$ gauge coupling.

By decomposing the complex scalar field ϕ into their real and imaginary components,

$$\phi = \langle \phi \rangle + \frac{1}{\sqrt{2}} (\varphi_r + i\varphi_i), \quad (20)$$

the masses of these fields are found to be

$$m_{\varphi_r} = 2\sqrt{\lambda_\phi} \langle \phi \rangle, \quad (21)$$

$$m_{\varphi_i} = 0, \quad (22)$$

respectively. Note that φ_i is a massless Nambu-Goldstone boson that can be absorbed by Z' in the unitary gauge. For the case of χ , after the decomposition

$$\chi = \frac{1}{\sqrt{2}} (\chi_r + i\chi_i), \quad (23)$$

the mass matrix for these real scalar fields is obtained:

$$\frac{1}{2} \begin{pmatrix} \chi_r & \chi_i \end{pmatrix} M_\chi^2 \begin{pmatrix} \chi_r \\ \chi_i \end{pmatrix} = \frac{1}{2} \begin{pmatrix} \chi_r & \chi_i \end{pmatrix} \begin{pmatrix} m_\chi'^2 + (r + r^*) \langle \phi \rangle & i(r - r^*) \langle \phi \rangle \\ i(r - r^*) \langle \phi \rangle & m_\chi'^2 - (r + r^*) \langle \phi \rangle \end{pmatrix} \begin{pmatrix} \chi_r \\ \chi_i \end{pmatrix}, \quad (24)$$

where

$$m_\chi'^2 = m_\chi^2 + \lambda_{\chi H} \langle H \rangle^2 + \lambda_{\phi\chi} \langle \phi \rangle^2. \quad (25)$$

In the simple case where the coupling r is real, the matrix M_χ^2 is diagonal, and the masses of the particles χ_r and χ_i are respectively

$$m_{\chi_r} = m_\chi'^2 + 2r \langle \phi \rangle, \quad (26)$$

$$m_{\chi_i} = m_\chi'^2 - 2r \langle \phi \rangle. \quad (27)$$

Since the field χ does not develop a nonzero VEV, there is no mass mixing between the SM leptons and the vector-like ones. However, the situation for quarks is more involved because the VEV of ϕ generates mass mixing terms via the new Yukawa interactions with the couplings $w = (w_1, w_2, w_3)$ in Eq. (14). To diagonalize the quark mass matrices, M^u and M^d , we need to use four 4×4 unitary matrices to transform the quark gauge eigenstates, (u^1, u^2, u^3, U) and (d^1, d^2, d^3, D) , into the mass eigenstates, (u, c, t, \mathcal{U}) and (d, s, b, \mathcal{D}) :

$$\begin{pmatrix} u_{L,R} \\ c_{L,R} \\ t_{L,R} \\ \mathcal{U}_{L,R} \end{pmatrix} = (V_{L,R}^u)_{4 \times 4} \begin{pmatrix} u_{L,R}^1 \\ u_{L,R}^2 \\ u_{L,R}^3 \\ U_{L,R} \end{pmatrix}, \quad \begin{pmatrix} d_{L,R} \\ s_{L,R} \\ b_{L,R} \\ \mathcal{D}_{L,R} \end{pmatrix} = (V_{L,R}^d)_{4 \times 4} \begin{pmatrix} d_{L,R}^1 \\ d_{L,R}^2 \\ d_{L,R}^3 \\ D_{L,R} \end{pmatrix}. \quad (28)$$

The diagonal mass matrices of up-type and down-type quarks then read

$$M_{\text{diag}}^u = V_L^u M^u (V_R^u)^\dagger, \quad (29)$$

$$M_{\text{diag}}^d = V_L^d M^d (V_R^d)^\dagger. \quad (30)$$

2.2 The gauge kinetic mixing

In a model with two Abelian gauge symmetries, the gauge kinetic mixing term of the form $-\frac{k}{2} F_{\mu\nu}^1 F^{2\mu\nu}$ can be introduced in the Lagrangian without violating any symmetry [32]. Here, $F_{\mu\nu}^1$, $F^{2\mu\nu}$ and k are respectively the field strength tensors of the $U(1)_Y$ and $U(1)_X$ gauge fields and the kinetic mixing coefficient. In fact, the gauge kinetic mixing term is always generated radiatively [33], even though it is set to zero at high energy scales [34]. In the presence of such term, the gauge kinetic part of the Lagrangian relating to the Abelian groups can be written as

$$\mathcal{L}_{\text{kinetic}}^{\text{gauge}} \supset -\frac{1}{4} \begin{pmatrix} F_{\mu\nu}^1 & F_{\mu\nu}^2 \end{pmatrix} \begin{pmatrix} 1 & k \\ k & 1 \end{pmatrix} \begin{pmatrix} F^{1\mu\nu} \\ F^{2\mu\nu} \end{pmatrix}. \quad (31)$$

By an appropriate transformation in the space of the Abelian gauge fields, the kinetic Lagrangian can be made canonical. In the new basis, the covariant derivative is then expressed

as

$$D_\mu \supset \partial_\mu - iY g_Y B_\mu - iX' g'_X \mathcal{Z}'_\mu, \quad (32)$$

where the new charge X' and the new gauge coupling g'_X are determined by the original quantities and the kinetic mixing coefficient k as

$$X' = \frac{-k g_Y}{g_X} Y + X, \quad (33)$$

$$g'_X = \frac{g_X}{\sqrt{1 - k^2}}. \quad (34)$$

Here, $Y(X)$ and $g_Y(g_X)$ are the charge and the gauge coupling corresponding to the Abelian group $U(1)_Y(U(1)_X)$, respectively. The nonzero kinetic mixing coefficient k induces a shift in the $U(1)_X$ charge and modifies the relevant gauge coupling.

After the electroweak symmetry breaking by the VEV of the SM Higgs field, $\langle H \rangle$, the kinetic coefficient generates a mass mixing between the \mathcal{Z} and \mathcal{Z}' bosons, leading to a non-diagonal mass matrix for these particles:

$$M_{\mathcal{Z}\mathcal{Z}'}^2 = \begin{pmatrix} (g_2^2 + g_Y^2) \frac{\langle H \rangle^2}{2} & -X'_H g'_X \sqrt{g_2^2 + g_Y^2} \langle H \rangle^2 \\ -X'_H g'_X \sqrt{g_2^2 + g_Y^2} \langle H \rangle^2 & 2g_X'^2 (X_H'^2 \langle H \rangle^2 + X_\phi'^2 \langle \phi \rangle^2) \end{pmatrix}. \quad (35)$$

To diagonalize the above mass matrix, we use the following orthogonal rotation:

$$\begin{pmatrix} \mathcal{Z}_\mu \\ \mathcal{Z}'_\mu \end{pmatrix} = \begin{pmatrix} \cos \alpha_Z & -\sin \alpha_Z \\ \sin \alpha_Z & \cos \alpha_Z \end{pmatrix} \begin{pmatrix} Z_\mu \\ Z'_\mu \end{pmatrix}, \quad (36)$$

where Z and Z' are the mass eigenstates, and the mixing angle α_Z is determined as

$$\tan 2\alpha_Z = \frac{2(M_{\mathcal{Z}\mathcal{Z}'}^2)_{12}}{(M_{\mathcal{Z}\mathcal{Z}'}^2)_{11} - (M_{\mathcal{Z}\mathcal{Z}'}^2)_{22}}. \quad (37)$$

It is worth noticing that, in the limit of no kinetic mixing ($k = 0$), the pure BDW model is recovered, namely $X' = X$, $g'_X = g_X$, and $\alpha_Z = 0$.

From the covariant derivative of muon, we find the interaction terms between the muon and the Z and Z' bosons as

$$\begin{aligned} \mathcal{L} \supset & \bar{\mu} \left[(g_V \cos \alpha_Z + g_V^k \sin \alpha_Z) \gamma^\mu + (g_A \cos \alpha_Z + g_A^k \sin \alpha_Z) \gamma^\mu \gamma^5 \right] \mu Z_\mu + \\ & \bar{\mu} \left[(-g_V \sin \alpha_Z + g_V^k \cos \alpha_Z) \gamma^\mu + (-g_A \sin \alpha_Z + g_A^k \cos \alpha_Z) \gamma^\mu \gamma^5 \right] \mu Z'_\mu, \end{aligned} \quad (38)$$

where

$$g_V = \frac{g_2}{\cos \theta_W} \left(-\frac{1}{4} + \sin^2 \theta_W \right), \quad (39)$$

$$g_A = \frac{g_2}{4 \cos \theta_W}, \quad (40)$$

$$X'_{\mu_L} = \frac{-kg_Y}{g_X} Y_{\mu_L} = \frac{kg_Y}{2g_X}, \quad (41)$$

$$X'_{\mu_R} = \frac{-kg_Y}{g_X} Y_{\mu_R} = \frac{kg_Y}{g_X}, \quad (42)$$

$$g_V^k = g'_X \frac{X'_{\mu_L} + X'_{\mu_R}}{2} = \frac{3kg_Y}{4\sqrt{1-k^2}}, \quad (43)$$

$$g_A^k = g'_X \frac{-X'_{\mu_L} + X'_{\mu_R}}{2} = \frac{kg_Y}{4\sqrt{1-k^2}}. \quad (44)$$

In the limit of no kinetic mixing, muons interact only with the Z boson just as in the SM. Similarly, the interaction terms between the new charged lepton E_R and these two massive neutral gauge bosons are obtained as

$$\begin{aligned} \mathcal{L} \supset & \left[\frac{g_2 \cos \alpha_Z}{\cos \theta_W} \left(-\frac{1}{2} + \sin^2 \theta_W \right) + g'_X X'_{L_R} \sin \alpha_Z \right] \overline{E_R} \gamma^\mu E_R Z_\mu \\ & + \left[-\frac{g_2 \sin \alpha_Z}{\cos \theta_W} \left(-\frac{1}{2} + \sin^2 \theta_W \right) + g'_X X'_{L_R} \cos \alpha_Z \right] \overline{E_R} \gamma^\mu E_R Z'_\mu, \end{aligned} \quad (45)$$

where

$$X'_{L_R} = \frac{-kg_Y}{g_X} Y_{L_R} + X_{L_R} = \frac{kg_Y}{2g_X} + 1. \quad (46)$$

For the new scalar sector, the derivation of Z' and Z couplings with $\chi_{r,i}$ from their covariant derivatives leads to

$$\mathcal{L} \supset g'_X X'_\chi \sin \alpha_Z Z^\mu (\partial_\mu \chi_r \cdot \chi_i - \chi_r \cdot \partial_\mu \chi_i) + g'_X X'_\chi \cos \alpha_Z Z'^\mu (\partial_\mu \chi_r \cdot \chi_i - \chi_r \cdot \partial_\mu \chi_i), \quad (47)$$

where $X'_\chi = X_\chi = -1$.

The flavor changing neutral currents (FCNCs) in the quark sector are induced at the tree level due to the mixing between the SM quarks and the vector-like quarks. We parameterize the couplings between the b -quark, the s -quark and the massive neutral gauge bosons as follows

$$\begin{aligned} \mathcal{L} \supset & X'_b g'_X (A_{bs} \overline{b_L} \gamma^\mu s_L + B_{bs} \overline{b_R} \gamma^\mu s_R) \mathcal{Z}'_\mu + \frac{g_2}{\cos \theta_W} C_{bs} \overline{b_R} \gamma^\mu s_R \mathcal{Z}_\mu + h.c. \\ = & \left[(X'_b g'_X A_{bs} \sin \alpha_Z) \overline{b_L} \gamma^\mu s_L + \left(X'_b g'_X B_{bs} \sin \alpha_Z + \frac{g_2}{\cos \theta_W} C_{bs} \cos \alpha_Z \right) \overline{b_R} \gamma^\mu s_R \right] Z_\mu + \\ & \left[(X'_b g'_X A_{bs} \cos \alpha_Z) \overline{b_L} \gamma^\mu s_L + \left(X'_b g'_X B_{bs} \cos \alpha_Z - \frac{g_2}{\cos \theta_W} C_{bs} \sin \alpha_Z \right) \overline{b_R} \gamma^\mu s_R \right] Z'_\mu + h.c., \end{aligned} \quad (48)$$

where

$$X'_b \equiv X'_c = -2 - \frac{kg_Y}{6g_X}, \quad (49)$$

and the parameters A_{bs} , B_{bs} and C_{bs} characterize the FCNCs in the $b \rightarrow s$ transition. At the tree level, these parameters are determined as

$$A_{bs} = \left(V_L^d \cdot \text{Diag}(0, 0, 0, 1) \cdot V_L^{d\dagger} \right)_{32} = (V_L^d)_{34} (V_L^d)_{24}^*, \quad (50)$$

$$B_{bs} = \left(V_R^d \cdot \text{Diag}(0, 0, 0, 1) \cdot V_R^{d\dagger} \right)_{32} = (V_R^d)_{34} (V_R^d)_{24}^*, \quad (51)$$

$$C_{bs} = \left(V_R^d \cdot \text{Diag} \left(\frac{1}{3} \sin^2 \theta_W, \frac{1}{3} \sin^2 \theta_W, \frac{1}{3} \sin^2 \theta_W, -\frac{1}{2} + \frac{1}{3} \sin^2 \theta_W \right) \cdot V_R^{d\dagger} \right)_{32}. \quad (52)$$

Assuming that the mixing between the vector-like quarks and the first generation quarks is negligible for simplicity, the parameter C_{bs} can be approximated as

$$C_{bs} \approx \left(-\frac{1}{2} + \frac{1}{3} \sin^2 \theta_W \right) B_{bs}. \quad (53)$$

At the loop-level, these parameters are considered to be the effective couplings encoding the new physics relevant to the quark sector.

3 New physics contributions to muon $g - 2$ and Wilson coefficients

3.1 Muon $g - 2$

In this model, new physics contributes to the muon anomalous magnetic moment via the gauge interaction associated with the massive boson Z' , and the new Yukawa interaction between the scalar χ , the right-handed lepton E_R and the muon. The Feynman diagrams corresponding to the leading new physics contributions to the muon $g - 2$ are shown in Figure 1. The diagrams (a) and (b) in this figure are due to the Yukawa coupling y_μ in Eq. (14). The contribution related to the diagram (c) is generated from the gauge kinetic mixing effect.

From the matrix elements of these one-loop diagrams, after performing some algebraic calculation, we obtain the following expression for the new physics contributions to the muon $g - 2$:

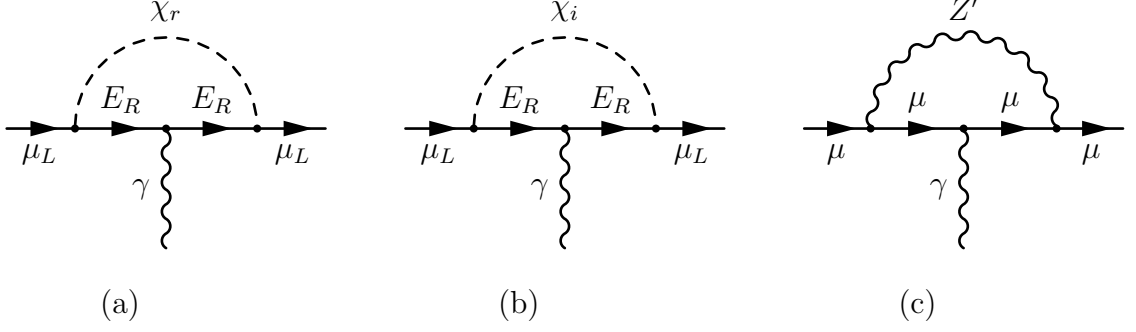


Figure 1: Leading new physics contributions to the muon $g - 2$.

$$\begin{aligned}
\Delta a_\mu^{\text{NP}} = & \frac{|y_\mu|^2 m_\mu^2}{32\pi^2 m_{\chi_r}^2} \left[F_g(\tau) + \left(\frac{1}{1+\delta} \right) F_g \left(\frac{\tau}{1+\delta} \right) \right] \\
& + \frac{\beta}{4\pi^2} \int_0^1 dz (1-z) \left\{ \left(-g_A \sin \alpha_Z + g_A^k \cos \alpha_Z \right)^2 (3z-1) \ln [\beta(1-z)^2 + z] \right. \\
& \left. + \frac{\left(-g_V \sin \alpha_Z + g_V^k \cos \alpha_Z \right)^2 z(1-z) - \left(-g_A \sin \alpha_Z + g_A^k \cos \alpha_Z \right)^2 z(z+3)}{\beta(1-z)^2 + z} \right\},
\end{aligned} \tag{54}$$

where

$$\tau = \frac{m_L^2}{m_{\chi_r}^2}, \tag{55}$$

$$\delta = \frac{m_{\chi_i}^2}{m_{\chi_r}^2} - 1, \tag{56}$$

$$\beta = \frac{m_\mu^2}{m_{Z'}^2}. \tag{57}$$

The first term in Eq. (54) with the squared brackets corresponds to the new physics contributions in Figures 1a and 1b. Here, the loop function $F_g(x)$ is defined as

$$F_g(x) = \frac{1}{6(1-x)^4} (6x \ln x + x^3 - 6x^2 + 3x + 2). \tag{58}$$

This term is in agreement with the result in Ref. [30] for the case of no kinetic mixing. The second term in Eq. (54) with the integral results from the effect of the gauge kinetic mixing via the diagram in Figure 1c. It vanishes in the limit $k = 0$.

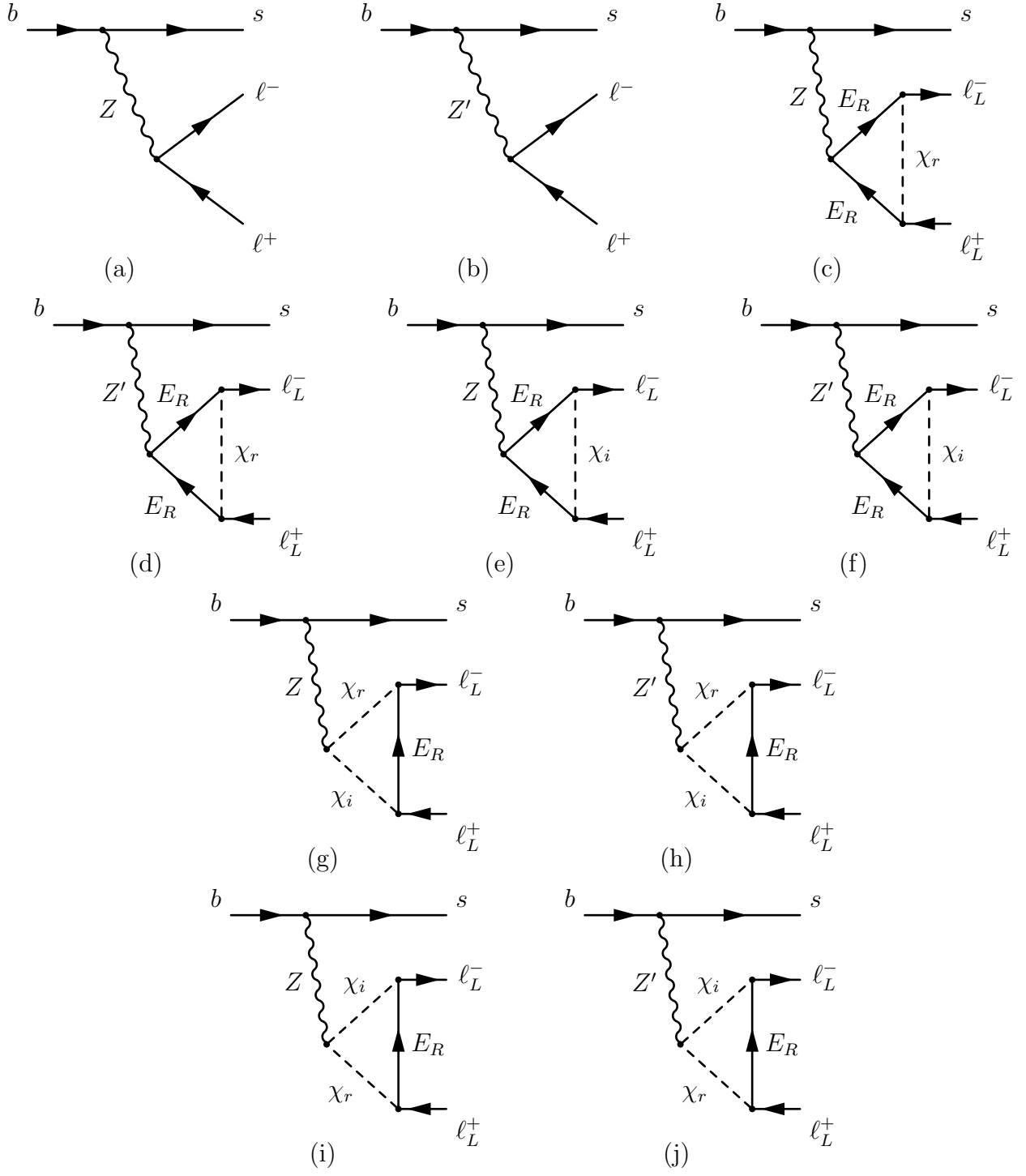


Figure 2: Leading new physics contributions to the Wilson coefficients $C_9^{(\prime)}$ and $C_{10}^{(\prime)}$.

3.2 Wilson coefficients

Since the scalar and pseudoscalar Wilson coefficients ($C_{S,P}$) are severely restricted by the leptonic decay $B_s \rightarrow \mu^+ \mu^-$ [19], in this subsection we consider the Wilson coefficients $C_{9,10}^{(\prime)}$ to be used for the calculation of the semileptonic branching ratios of B mesons. The leading new physics contributions to the Wilson coefficients $C_9^{(\prime)}$ and $C_{10}^{(\prime)}$ are depicted by the Feynman diagrams in Figure 2. Here, we consider the diagrams whose the matrix elements are proportional to the second order of the gauge couplings g_2 or g_X .

In Figure 2a, the new physics enters this tree-level diagram only via the coupling of the bsZ vertex resulting from the mixing between the SM quarks and the vector-like quarks. The contribution according to the diagram 2b is due to the gauge kinetic mixing effect. The contributions due to the diagrams (c)-(f) stem from the gauge interactions of the vector-like charged lepton E_R with both Z and Z' bosons. The cases for the diagrams (g)-(j) relevant to the gauge interactions of the scalars $\chi_{r,i}$ are more involved. While the contributions from the diagrams (h) and (j) always exist, those from the diagrams (g) and (i) are due to the ZZ' mixing that only emerges when $k \neq 0$.

The new physics contributions to the Wilson coefficients $C_{9,10}^{(\prime)}$ according to the diagrams in Figure 2 are expressed as

$$C_9^{\text{NP}} = \frac{12g_X + kg_Y}{12(1-k^2)} \left(\frac{g_X \cos \alpha_Z}{m_{Z'}^2} A_k + \frac{g_2 \sin \alpha_Z}{m_Z^2} A_k^Z \right) \Lambda_{\text{SM}}^2 \frac{|V_{tb} V_{ts}^*|}{V_{tb} V_{ts}^*} A_{bs}, \quad (59)$$

$$C_9^{\text{NP}} = \left\{ \frac{12g_X + kg_Y}{12(1-k^2)} \left(\frac{g_X \cos \alpha_Z}{m_{Z'}^2} A_k + \frac{g_2 \sin \alpha_Z}{m_Z^2} A_k^Z \right) + \frac{g_2 \left(-\frac{1}{2} + \frac{1}{3} \sin^2 \theta_W \right)}{2 \cos \theta_W \sqrt{1-k^2}} \left[\frac{g_X \sin \alpha_Z}{m_{Z'}^2} A_k - \frac{g_2 \cos \alpha_Z}{m_Z^2} A_k^Z \right] \right\} \Lambda_{\text{SM}}^2 \frac{|V_{tb} V_{ts}^*|}{V_{tb} V_{ts}^*} B_{bs}, \quad (60)$$

$$C_{10}^{\text{NP}} = \frac{12g_X + kg_Y}{12(1-k^2)} \left(\frac{g_X \cos \alpha_Z}{m_{Z'}^2} B_k + \frac{g_2 \sin \alpha_Z}{m_Z^2} B_k^Z \right) \Lambda_{\text{SM}}^2 \frac{|V_{tb} V_{ts}^*|}{V_{tb} V_{ts}^*} A_{bs}, \quad (61)$$

$$C_{10}^{\text{NP}} = \left\{ \frac{12g_X + kg_Y}{12(1-k^2)} \left(\frac{g_X \cos \alpha_Z}{m_{Z'}^2} B_k + \frac{g_2 \sin \alpha_Z}{m_Z^2} B_k^Z \right) + \frac{g_2 \left(-\frac{1}{2} + \frac{1}{3} \sin^2 \theta_W \right)}{2 \cos \theta_W \sqrt{1-k^2}} \left[\frac{g_X \sin \alpha_Z}{m_{Z'}^2} B_k - \frac{g_2 \cos \alpha_Z}{m_Z^2} B_k^Z \right] \right\} \Lambda_{\text{SM}}^2 \frac{|V_{tb} V_{ts}^*|}{V_{tb} V_{ts}^*} B_{bs}, \quad (62)$$

where the intermediate notations A_k , A_k^Z , B_k , and B_k^Z are defined as follows

$$A_k(q^2) = \left[\frac{3kg_Y \cos \alpha_Z}{4g_X} - \frac{g_2 \sqrt{1-k^2} \sin \alpha_Z}{g_X \cos \theta_W} \left(-\frac{1}{4} + \sin^2 \theta_W \right) \right] + \frac{|y_\ell|^2 \cos \alpha_Z}{32\pi^2} f_A + \frac{|y_\ell|^2}{32\pi^2} \left[\left(1 + \frac{kg_Y}{2g_X} \right) \cos \alpha_Z - \frac{g_2 \sqrt{1-k^2} \sin \alpha_Z}{g_X \cos \theta_W} \left(-\frac{1}{2} + \sin^2 \theta_W \right) \right] g_A, \quad (63)$$

$$A_k^Z(q^2) = \left[\frac{\sqrt{1-k^2}}{\cos \theta_W} \left(-\frac{1}{4} + \sin^2 \theta_W \right) \cos \alpha_Z + \frac{3kg_Y}{4g_2} \sin \alpha_Z \right] + \frac{|y_\ell|^2 g_X \sin \alpha_Z}{32\pi^2 g_2} f_A \\ + \frac{|y_\ell|^2}{32\pi^2} \left[\frac{\sqrt{1-k^2} \cos \alpha_Z}{\cos \theta_W} \left(-\frac{1}{2} + \sin^2 \theta_W \right) + \left(1 + \frac{kg_Y}{2g_X} \right) \frac{g_X \sin \alpha_Z}{g_2} \right] g_A, \quad (64)$$

$$B_k(q^2) = \left[\frac{kg_Y \cos \alpha_Z}{4g_X} - \frac{g_2 \sqrt{1-k^2} \sin \alpha_Z}{4g_X \cos \theta_W} \right] - \frac{|y_\ell|^2 \cos \alpha_Z}{32\pi^2} f_B \\ + \frac{|y_\ell|^2}{32\pi^2} \left[\left(1 + \frac{kg_Y}{2g_X} \right) \cos \alpha_Z - \frac{g_2 \sqrt{1-k^2} \sin \alpha_Z}{g_X \cos \theta_W} \left(-\frac{1}{2} + \sin^2 \theta_W \right) \right] g_B, \quad (65)$$

$$B_k^Z(q^2) = \left[\frac{\sqrt{1-k^2}}{4 \cos \theta_W} \cos \alpha_Z + \frac{kg_Y}{4g_2} \sin \alpha_Z \right] - \frac{|y_\ell|^2 g_X \sin \alpha_Z}{32\pi^2 g_2} f_B \\ + \frac{|y_\ell|^2}{32\pi^2} \left[\frac{\sqrt{1-k^2} \cos \alpha_Z}{\cos \theta_W} \left(-\frac{1}{2} + \sin^2 \theta_W \right) + \left(1 + \frac{kg_Y}{2g_X} \right) \frac{g_X \sin \alpha_Z}{g_2} \right] g_B. \quad (66)$$

In these above formulas, the loop functions f_A , g_A , f_B , and g_B are given by

$$f_A = \int dx dy dz \delta(1-x-y-z) \left\{ \frac{\ln[(\tau z + x + y + \delta x)(\tau z + x + y + \delta y)]}{2} \right. \\ \left. - \frac{m_\ell^2}{m_{\chi_r}^2} z(1-z) \left[\frac{1}{\tau z + x + y + \delta x} + \frac{1}{\tau z + x + y + \delta y} \right] \right\}, \quad (67)$$

$$g_A = \int dx dy dz \delta(1-x-y-z) \left\{ -\frac{\ln[(\tau(x+y)+z)(\tau(x+y)+z+\delta z)]}{2} \right. \\ \left. + \frac{z^2 m_\ell^2 + xyq^2 + m_L^2}{2m_{\chi_r}^2} \left[\frac{1}{\tau(x+y)+z} + \frac{1}{\tau(x+y)+z+\delta z} \right] \right\}, \quad (68)$$

$$f_B = \int dx dy dz \delta(1-x-y-z) \frac{\ln[(\tau z + x + y + \delta x)(\tau z + x + y + \delta y)]}{2}, \quad (69)$$

$$g_B = \int dx dy dz \delta(1-x-y-z) \left\{ \frac{\ln[(\tau(x+y)+z)(\tau(x+y)+z+\delta z)]}{2} \right. \\ \left. + \frac{z^2 m_\ell^2 - xyq^2 - m_L^2}{2m_{\chi_r}^2} \left[\frac{1}{\tau(x+y)+z} + \frac{1}{\tau(x+y)+z+\delta z} \right] \right\}, \quad (70)$$

as the results of the Feynman parameterization. In these formulas, ℓ is one of the SM charge leptons $\{e, \mu, \tau\}$.

4 Numerical analysis

In this section, we consider the phenomenological constraints including the muon anomalous magnetic moments, and the rare semileptonic decays of B mesons. The current deviation

between the experimental value and the SM prediction of muon $g - 2$ is [1, 2]

$$\Delta a_\mu \equiv a_\mu^{\text{exp}} - a_\mu^{\text{SM}} = (28.1 \pm 7.6) \times 10^{-10}, \quad (71)$$

The on-going E989 experiment will be able to reach a precision of 140 parts-per-billion [3]. Assuming the same center value of Δa_μ as the current result (71), the projected difference between the SM prediction and the experimental value reads

$$\Delta a_\mu^{\text{projected}} = (28.1 \pm 4.6) \times 10^{-10}, \quad (72)$$

corresponding to a 6.1σ deviation. For the B -meson semileptonic decays, we take into account the branching ratios of the processes $B^+ \rightarrow K^+ \mu^+ \mu^-$, $B^0 \rightarrow K^{*0} \mu^+ \mu^-$, and the observables, R_K and R_{K^*} , characterizing the violation of lepton flavor universality. For the muon invariant mass in the region $q^2 = [1.1, 6.0] \text{ GeV}^2$, the 2σ allowed ranges for the following B -meson observables are:

$$1.050 \times 10^{-7} < BR(B^+ \rightarrow K^+ \mu^+ \mu^-) < 1.322 \times 10^{-7}, \quad [35, 36] \quad (73)$$

$$1.382 \times 10^{-7} < BR(B^0 \rightarrow K^{*0} \mu^+ \mu^-) < 1.970 \times 10^{-7}, \quad [35, 37] \quad (74)$$

$$0.734 < R_K = \frac{BR(B^+ \rightarrow K^+ \mu^+ \mu^-)}{BR(B^+ \rightarrow K^+ e^+ e^-)} < 0.970, \quad [38, 7] \quad (75)$$

$$0.53 < R_{K^*} = \frac{BR(B^0 \rightarrow K^{*0} \mu^+ \mu^-)}{BR(B^0 \rightarrow K^{*0} e^+ e^-)} < 0.95, \quad [38, 8] \quad (76)$$

according to the updated results from the LHCb experiment.

In the numerical analysis, we assume, for simplicity, that the new vector-like leptons have sizable coupling with muons (y_μ), while the corresponding coupling with electrons (y_e) is negligible. Therefore, the set of relevant input parameters are

$$m_{\chi_r}, m_{Z'}, k, g_X, y_\mu, \tau, \delta, A_{bs}, B_{bs}. \quad (77)$$

The branching ratios of the B -meson decay processes are calculated using the methods described in Refs. [39, 40, 41]. The relevant form factors from Ref. [42] are employed in our calculation.

Constraints on m_{χ_r} :

Since the mass of the scalar field χ_r only appears as an independent parameter in Eq. (54), it is constrained by the bounds (71) on the new physics contributions to the muon $g - 2$. In Figure 3, we show the dependence of Δa_μ^{NP} on m_{χ_r} for fixed values of other inputs, $\tau = 1.1$, $\delta = 10$, $y_\mu = 2$, and $k = 0$. In this case, the current bounds on the muon $g - 2$ yield the 2σ allowed range for the χ_r mass to be $57 \text{ GeV} \lesssim m_{\chi_r} \lesssim 105 \text{ GeV}$. In the near future, when the measurement at the E989 experiment is completed, we expect that this range will be improved.

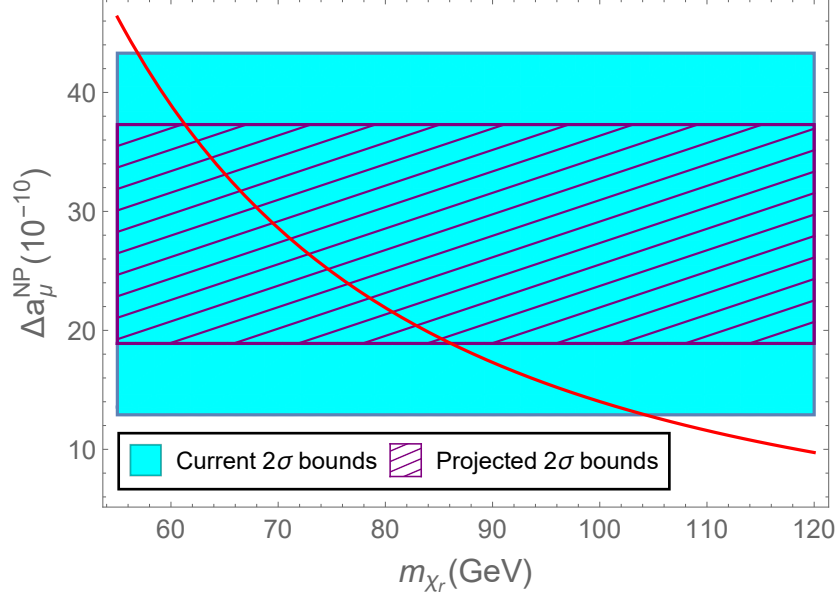


Figure 3: The new physics contributions to the muon anomalous magnetic moment as a function of m_{χ_r} for the case of $\tau = 1.1$, $\delta = 10$, $y_\mu = 2$, and $k = 0$.

The projected bounds in Eq. (72) imply more severe 2σ limits for this parameter that are $61 \text{ GeV} \lesssim m_{\chi_r} \lesssim 86 \text{ GeV}$. In the subsequent analysis regarding the muon $g - 2$, we choose $m_{\chi_r} = 70 \text{ GeV}$ as a representative value.

Constraints on (A_{bs}, B_{bs}) plane:

For the parameters A_{bs} and B_{bs} , they are constrained by the measurements of the branching fractions of the semileptonic decays $B^+ \rightarrow K^+ \mu^+ \mu^-$, and $B^0 \rightarrow K^{*0} \mu^+ \mu^-$ (Eqs. (73)-(74)), as well as the ratios measuring the lepton universality violation R_K and R_{K^*} (Eqs.(75)-(76)). In Figure 4, these constraints (represented by the red, yellow, blue and green colors, respectively) at the level of 2σ are depicted on the (A_{bs}, B_{bs}) plane for fixed values of other parameters $m_{Z'} = 150 \text{ GeV}$, $y_\mu = 2$, $g_X = 3$, $\tau = 1.1$, and $\delta = 10$, in the case of vanishing kinetic mixing. The strips corresponding to each of these constraints appear approximately in the elliptical forms. It is due to the fact that the relevant observables are quadratic functions of the Wilson coefficients, $C_9^{(')\text{NP}}$ and $C_{10}^{(')\text{NP}}$, that in turns are proportional to the first order of the parameters A_{bs} and B_{bs} . If the confident level of 3σ was taken into account there would be two regions on the left and on the right of the figure where these strips overlap. However, since we restrict to the 2σ level, the right region is marginally excluded. The region satisfying all these constraints is extracted and shown separately in Figure 5. We observe that the allowed ranges for A_{bs} and B_{bs} in this case are $8.2 \times 10^{-5} \lesssim A_{bs} \lesssim 11.3 \times 10^{-5}$, and $-6.8 \times 10^{-5} \lesssim B_{bs} \lesssim -1.6 \times 10^{-5}$, respectively. From the magnitudes of these two parameters, it is clearly that all the relevant

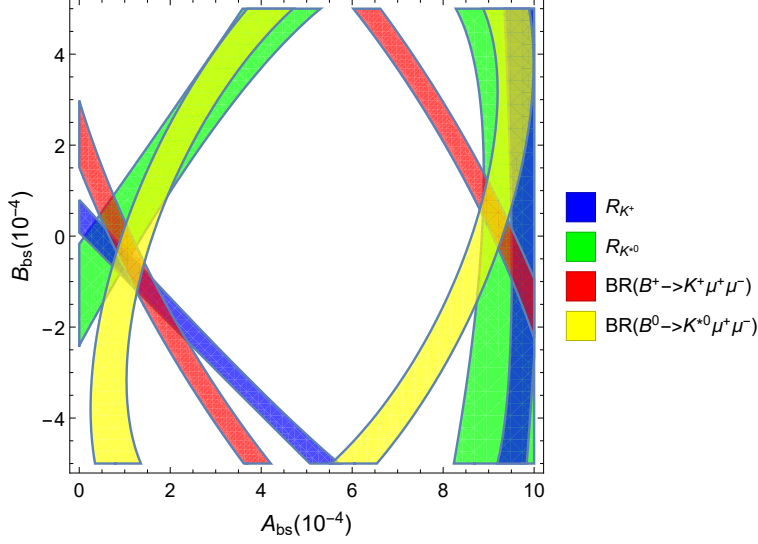


Figure 4: Phenomenological constraints on the (A_{bs}, B_{bs}) plane for the case of $m_{Z'} = 150$ GeV, $y_\mu = 2$, $g_X = 3$, $\tau = 1.1$, $\delta = 10$, and $k = 0$.

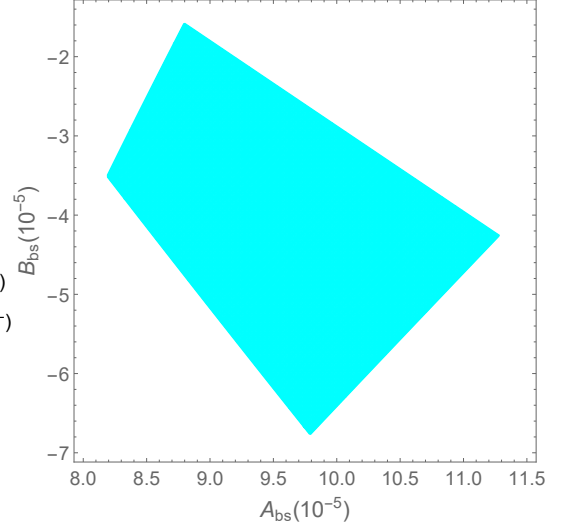


Figure 5: Viable parameter region on the (A_{bs}, B_{bs}) plane for the case of $m_{Z'} = 150$ GeV, $y_\mu = 2$, $g_X = 3$, $\tau = 1.1$, $\delta = 10$, and $k = 0$.

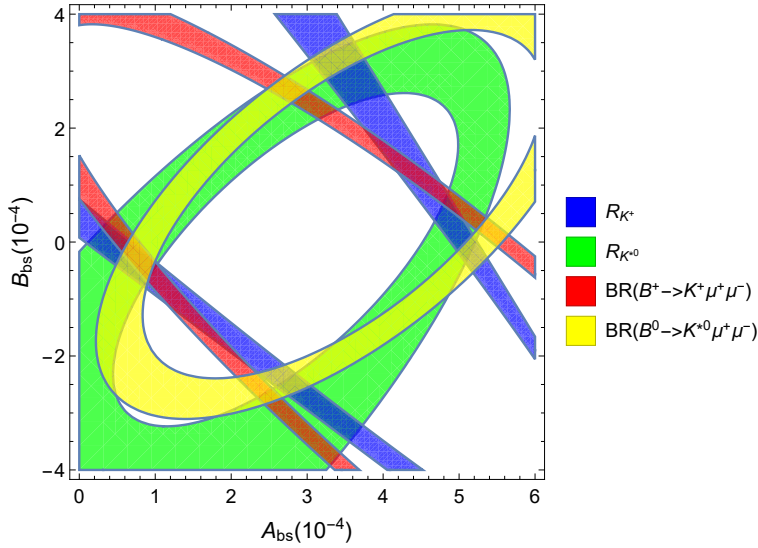


Figure 6: Phenomenological constraints on the (A_{bs}, B_{bs}) plane for the case of $m_{Z'} = 150$ GeV, $y_\mu = 2$, $g_X = 3$, $\tau = 1.1$, $\delta = 10$, and $k = 0.09$.

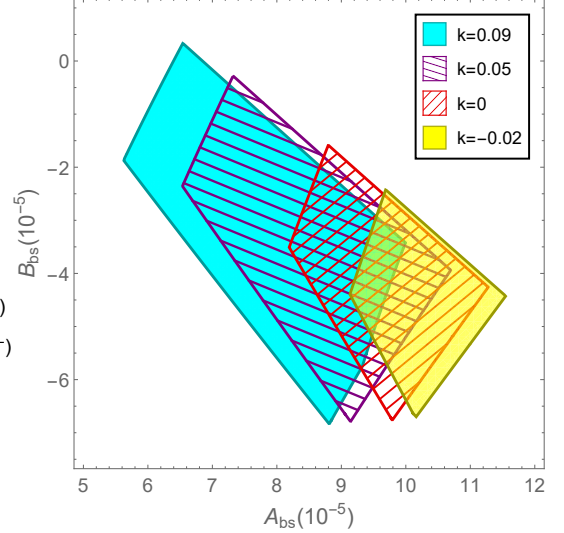


Figure 7: Viable parameter regions on the (A_{bs}, B_{bs}) plane for the case of $m_{Z'} = 150$ GeV, $y_\mu = 2$, $g_X = 3$, $\tau = 1.1$, $\delta = 10$, and various values of the kinetic mixing coefficient $k = -0.02, 0, 0.05, 0.09$.

FCNC processes are very much suppressed.

In Figure 6, we plot the same constraints as those in Figure 4 but with a nonzero kinetic mixing coefficient, $k = 0.09$. It is noteworthy that, in both cases with and without the kinetic

mixing, the branching fractions themselves play an equally important roles as the ratios R_K and R_K^* in the combination of phenomenological constraints to determine the allowed parameter region. Comparing these figures, we see that the allowed region for each constraint significantly changes once the gauge kinetic mixing effects are taken into account. As the result, the overlapped region is modified. In Figure 7, the regions satisfying all the considered constraints from B -meson decays are depicted for different scenarios with the kinetic mixing coefficient to be $k = -0.02, 0, 0.05$, and 0.09 . They are shown as the yellow, red slashed, purple back-slashed, and cyan regions in the plot. We observe that the viable region shifts to the left toward smaller values of A_{bs} , and extends upward when the kinetic mixing coefficient becomes larger. As the consequence, the windows for the parameters A_{bs} and B_{bs} become more relaxed for larger values of k .

Constraints on (τ, δ) plane:

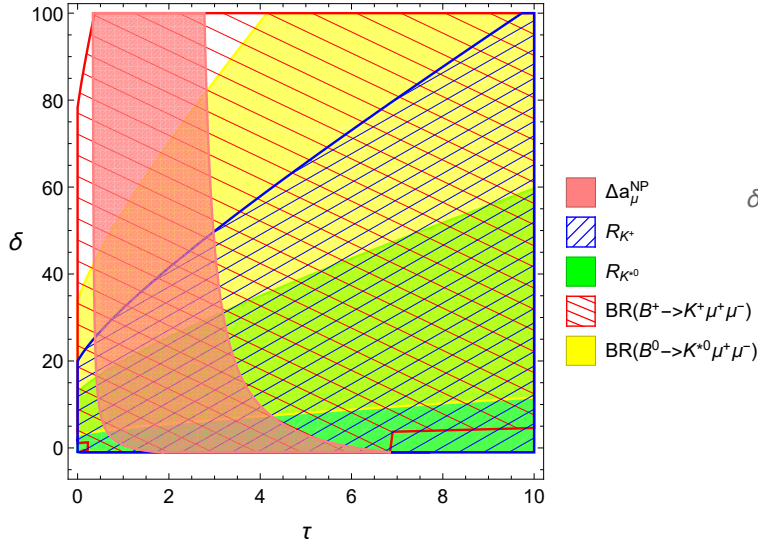


Figure 8: Phenomenological constraints on the (τ, δ) plane for the case of $m_{\chi_r} = 70$ GeV, $m_{Z'} = 150$ GeV, $y_\mu = 2$, $g_X = 3$, $A_{bs} = 9.5 \times 10^{-5}$, $B_{bs} = -4.0 \times 10^{-5}$, and $k = 0$.

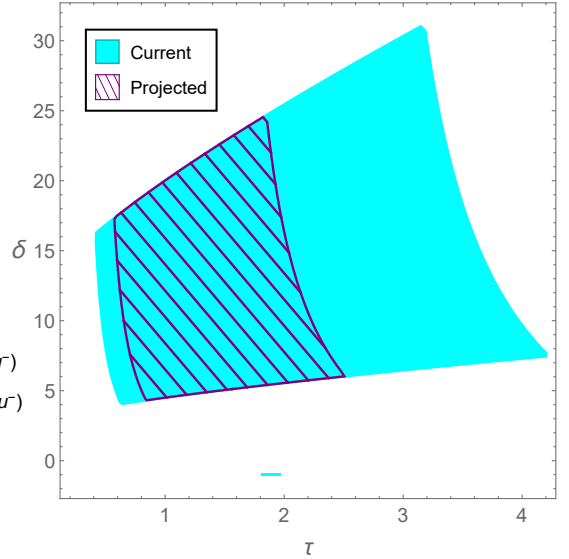


Figure 9: Viable parameter region on the (τ, δ) plane for the case of $m_{\chi_r} = 70$ GeV, $m_{Z'} = 150$ GeV, $y_\mu = 2$, $g_X = 3$, $A_{bs} = 9.5 \times 10^{-5}$, $B_{bs} = -4.0 \times 10^{-5}$, and $k = 0$. The hatched region corresponds to the projected result after the E989 experiment.

The parameters τ and δ involve in all the considered observables. Since δ is defined by the Eq. (56), it must satisfy the theoretical condition $\delta \geq -1$. In Figure 8, we show how the constraints on $\Delta a_\tau^{\text{NP}}$, R_K , R_{K^*} , $BR(B^+ \rightarrow K^+ \mu^+ \mu^-)$, and $BR(B^0 \rightarrow K^{*0} \mu^+ \mu^-)$ at the level of 2σ affect the (τ, δ) plane in the case with a vanishing kinetic mixing coefficient and fixed values of other inputs: $m_{\chi_r} = 70$ GeV, $m_{Z'} = 150$ GeV, $y_\mu = 2$, $g_X = 3$, $A_{bs} = 9.5 \times 10^{-5}$,

and $B_{bs} = -4.0 \times 10^{-5}$. We observe that most of the interested parameter region satisfies the constraint on $BR(B^+ \rightarrow K^+ \mu^+ \mu^-)$. The constraint on R_K is not severe as well in this particular case. The bounds on new physics contributions to the muon $g - 2$ require $0.3 \lesssim \tau \lesssim 3.2$ when $\delta \gtrsim 30$. It is because, for large values of δ , the second term in the squared bracket in Eq. (54) is negligible, and Δa_μ^{NP} depends mostly on the first term. As a consequence, the bounds on Δa_μ^{NP} specify the allowed range for τ that is almost independent of δ . However, this region with very large δ is roughly excluded by the experimental data on R_{K^*} . For δ smaller than about 30, the dependence of the allowed range of τ on δ becomes clearer. From this figure, beside the constraint on the muon $g - 2$, we see that those on R_{K^*} and the semileptonic branching ratio of the B^0 meson also play an important role in determining the 2σ allowed parameter region. In Figure 9, the region satisfying all these current bounds is shown in the cyan color. For the chosen set of other inputs, the allowed ranges for the two parameters are $0.4 \lesssim \tau \lesssim 4.2$ and $3.8 \lesssim \delta \lesssim 31.2$. When taking into account the projected result from the E989 experiment, the viable parameter region significantly shrinks by a factor of nearly one half. In particular, the expected range for these parameters are $0.6 \lesssim \tau \lesssim 2.5$ and $4.2 \lesssim \delta \lesssim 24.6$, respectively. This region is depicted by the hatched area in Figure 9.

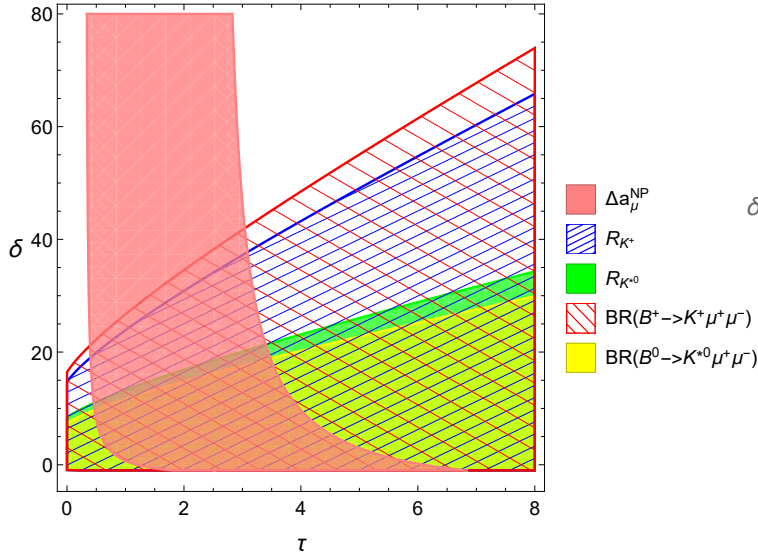


Figure 10: Phenomenological constraints on the (τ, δ) plane for the case of $m_{\chi_r} = 70$ GeV, $m_{Z'} = 150$ GeV, $y_\mu = 2$, $g_X = 3$, $A_{bs} = 9.5 \times 10^{-5}$, $B_{bs} = -4.0 \times 10^{-5}$, and $k = 0.09$.

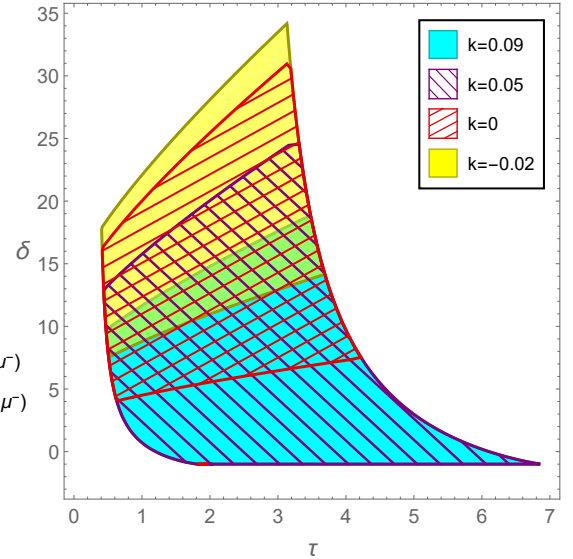


Figure 11: Viable parameter regions on the (τ, δ) plane for the case of $m_{\chi_r} = 70$ GeV, $m_{Z'} = 150$ GeV, $y_\mu = 2$, $g_X = 3$, $A_{bs} = 9.5 \times 10^{-5}$, $B_{bs} = -4.0 \times 10^{-5}$, and various values of the kinetic mixing coefficient $k = -0.02, 0, 0.05, 0.09$.

For nonzero kinetic mixing coefficients, the allowed parameter space gradually changes. In

Figure 10, the constraints are shown on the (τ, δ) plane for the same values of other parameters as the above case, but with $k = 0.09$. Comparing Figures 8 and 10, we observe that the nonzero kinetic mixing coefficient leads to smaller differences between the blue and the red hatched regions (constrained by the data on R_K and $BR(B^+ \rightarrow K^+ \mu^+ \mu^-)$), and between the green and the yellow regions (constrained by the data on R_{K^*} and $BR(B^0 \rightarrow K^{*0} \mu^+ \mu^-)$). In the meanwhile, the dependence of Δa_μ^{NP} on the gauge kinetic mixing is negligible for the interested values of k . For the case $k = 0.09$, the parameter region satisfying the bounds (74) also satisfies other bounds in Eqs. (73), (75) and (76). Therefore, the allowed region is determined by the 2σ constraints on Δa_μ^{NP} and the constraint on the branching ratio of the B^0 -meson decay. In Figure 11, the allowed regions on the (τ, δ) plane are plotted for various values of the kinetic mixing coefficient, namely $k = -0.02, 0, 0.06$, and 0.09 . Here, we see that when increasing k , the viable range for δ moves downward, while that for τ shifts to the right. This implies that, for a larger kinetic mixing coefficient, a smaller mass splitting between χ_i and χ_r is more favored, while a larger mass splitting between the vector-like leptons (N, E) and χ_r is more favored.

Constraints on the (g_X, y_μ) plane:

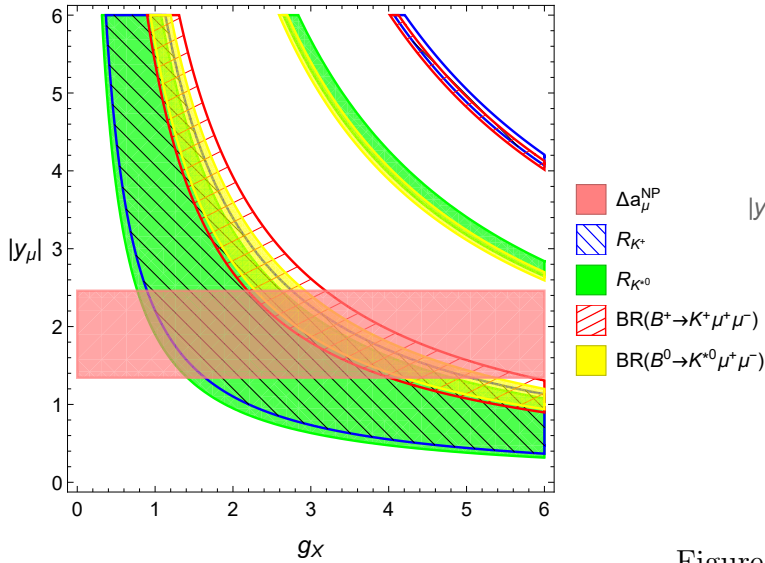


Figure 12: Phenomenological constraints on the (g_X, y_μ) plane for the case of $m_{\chi_r} = 70$ GeV, $m_{Z'} = 150$ GeV, $A_{bs} = 9.5 \times 10^{-5}$, $B_{bs} = -4.0 \times 10^{-5}$, $\tau = 1.1$, $\delta = 10$, and $k = 0$.

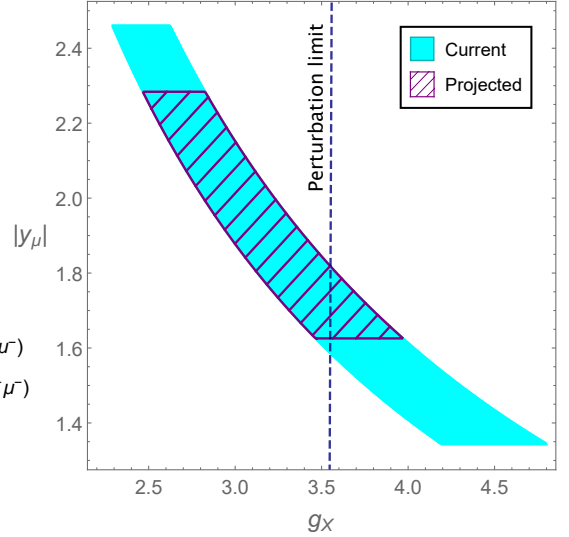


Figure 13: Viable parameter region on the (g_X, y_μ) plane for the case of $m_{\chi_r} = 70$ GeV, $m_{Z'} = 150$ GeV, $A_{bs} = 9.5 \times 10^{-5}$, $B_{bs} = -4.0 \times 10^{-5}$, $\tau = 1.1$, $\delta = 10$, and $k = 0$. The hatched region corresponds to the projected result after the E989 experiment.

In Figure 12, the phenomenological constraints are plotted on the (g_X, y_μ) plane in the case of no kinetic mixing and fixed values of other inputs, namely $m_{\chi_r} = 70$ GeV, $m_{Z'} = 150$ GeV,

$A_{bs} = 9.5 \times 10^{-5}$, $B_{bs} = -4.0 \times 10^{-5}$, $\tau = 1.1$, and $\delta = 10$. Since the muon $g - 2$ does not depend on the coupling g_X , the corresponding allowed region has the form of a horizontal band with $1.33 \lesssim |y_\mu| \lesssim 2.45$. We see that the muon $g - 2$ constraint is already more severe than the perturbation limit $y_\mu \lesssim \sqrt{4\pi}$. The parameter regions satisfying the constraints for other observables (R_K , R_{K^*} , and the branching ratios of B^+ and B^0 decays) have the hyperbolic forms. This is due to the Wilson coefficients $C_{9,10}^{(')\text{NP}}$ that define the correlation between g_X and y_μ for given values of the branching ratios. The viable region determined by all of the five phenomenological constraints is shown separately as the cyan region in Figure 13. To explain the anomalies on the B -meson decays, the new Yukawa coupling, y_μ , and the $U(1)_X$ gauge coupling, g_X , are required to have large values of $\mathcal{O}(1)$. Taking into account the perturbation limit for the $U(1)_X$ gauge coupling shown as the vertical blue dashed line in this figure, we observe that this theoretical condition excludes a large portion of the allowed parameter region. Although this is a constraint on the parameter g_X , it indirectly restricts the range of the parameter y_μ via their correlation. As the result, we have $2.27 \lesssim g_X \lesssim \sqrt{4\pi}$, and $1.58 \lesssim |y_\mu| \lesssim 2.46$. In the near future, the E989 experiment will impose a more severe constraint on the (g_X, y_μ) plane which is shown in hatched region. The projected bounds for these parameters are $2.46 \lesssim g_X \lesssim \sqrt{4\pi}$, and $1.62 \lesssim |y_\mu| \lesssim 2.28$, respectively.

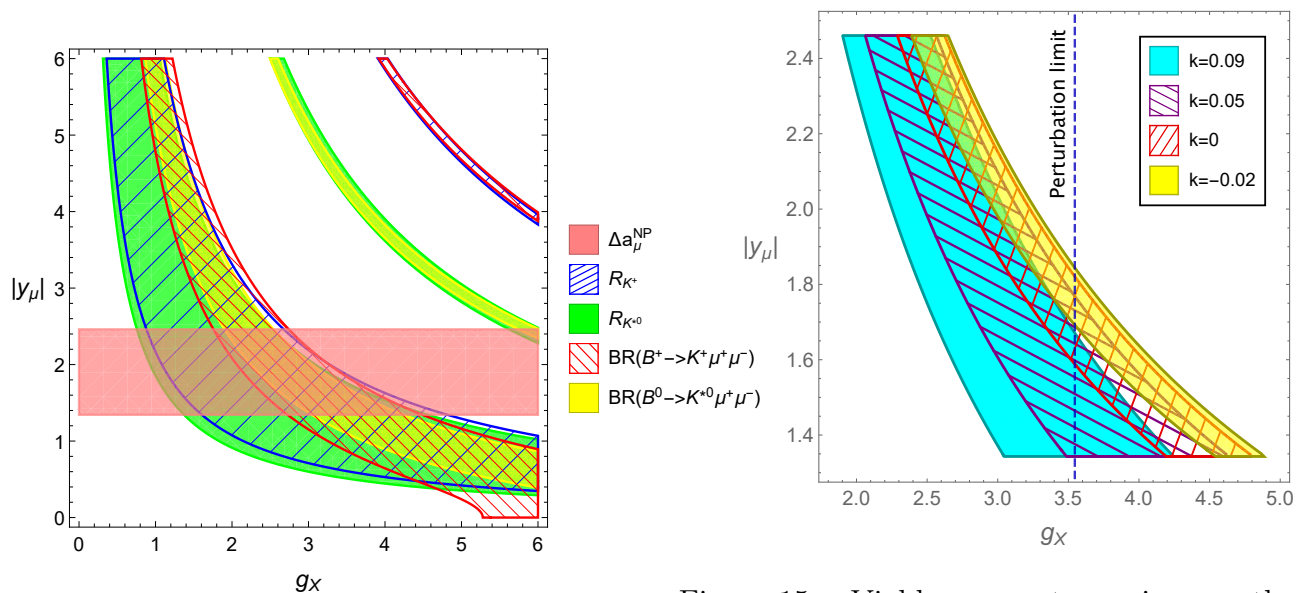


Figure 14: Phenomenological constraints on the (g_X, y_μ) plane for the case of $m_{\chi_r} = 70$ GeV, $m_{Z'} = 150$ GeV, $A_{bs} = 9.5 \times 10^{-5}$, $B_{bs} = -4.0 \times 10^{-5}$, $\tau = 1.1$, $\delta = 10$, and $k = 0.09$.

Figure 15: Viable parameter regions on the (g_X, y_μ) plane for the case of $m_{\chi_r} = 70$ GeV, $m_{Z'} = 150$ GeV, $A_{bs} = 9.5 \times 10^{-5}$, $B_{bs} = -4.0 \times 10^{-5}$, $\tau = 1.1$, $\delta = 10$, and various values of the kinetic mixing coefficient $k = -0.02, 0, 0.05, 0.09$.

For the case of nonzero kinetic mixing, the allowed regions are slightly changed as shown

in Figure 14 with $k = 0.09$ while other parameters are the same as in Figure 12. Since the effect of the kinetic mixing on the muon $g - 2$ is small, the allowed range determined from the Δa_μ^{NP} constraint remains almost intact. Although the constrained regions by the B -meson decay processes (the green, the yellow, the blue hatched and the red hatched regions) still have the hyperbolic shape as before, they slightly shift downward to the region with smaller values of y_μ (while the values of g_X are fixed) in comparison to the case of vanishing kinetic mixing. This is due to the additional contributions of the diagrams with the Z' -boson exchange at the tree level to the Wilson coefficients when $k \neq 0$. The viable parameter regions for various values of the gauge kinetic mixing coefficients ($k = -0.02, 0, 0.05$, and 0.09) are presented in Figure 15. When increasing k , the viable regions shift to the left. This implies that, for larger values of k , smaller values of g_X is more preferable when y_μ is fixed. Hence, it is obvious that the perturbation limit is less severe for a larger kinetic mixing coefficient. In this figure, taking into account the requirement from the perturbation theory on g_X , we observe that the viable regions become larger when increasing k . In particular, the lower bound for g_X reduces from 2.39 for $k = -0.02$ to 1.89 for $k = 0.09$, and the lower bound for $|y_\mu|$ reduces from 1.68 for $k = -0.02$ to 1.34 for $k = 0.09$. It is worth noticing that the upper bounds for g_X and $|y_\mu|$ are almost independent of k because they are determined from the perturbation requirement and the muon $g - 2$ constraint that are not sensitive to the gauge kinetic mixing.

Constraints on the $(g_X, m_{Z'})$ plane:

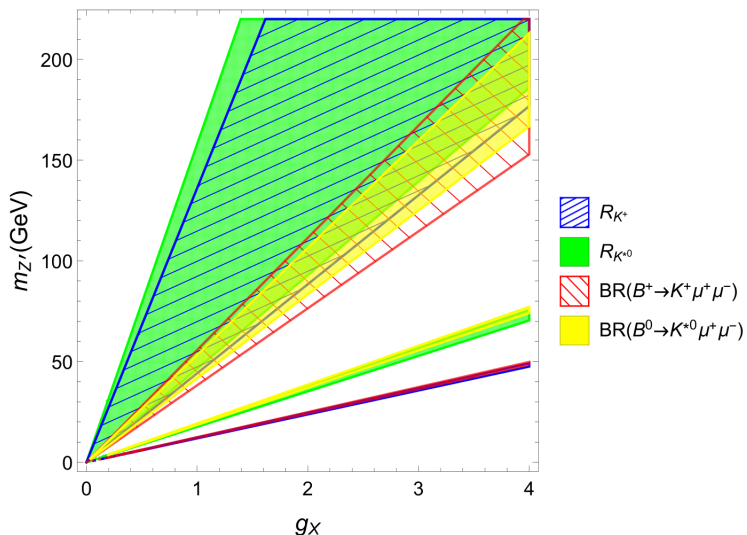


Figure 16: Phenomenological constraints on the $(g_X, m_{Z'})$ plane for the case of $y_\mu = 2$, $A_{bs} = 9.5 \times 10^{-5}$, $B_{bs} = -4.0 \times 10^{-5}$, $\tau = 1.1$, $\delta = 10$, and $k = 0$.

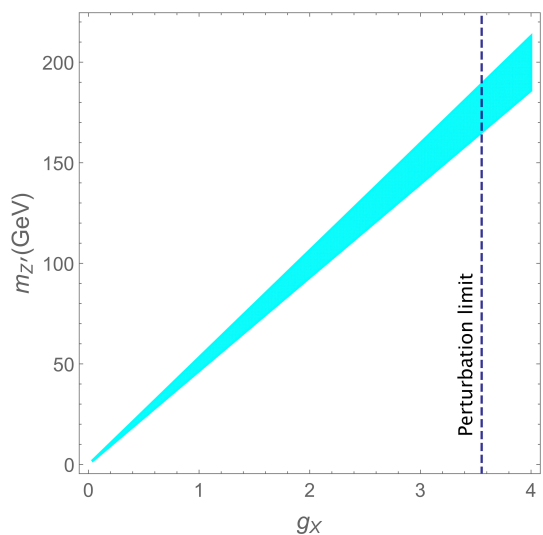


Figure 17: Viable parameter region on the $(g_X, m_{Z'})$ plane for the case of $y_\mu = 2$, $A_{bs} = 9.5 \times 10^{-5}$, $B_{bs} = -4.0 \times 10^{-5}$, $\tau = 1.1$, $\delta = 10$, and $k = 0$.

The phenomenological constraints on the $(g_X, m_{Z'})$ plane are presented in Figure 16 for the case of vanishing kinetic mixing and fixed values of other parameters as $y_\mu = 2$, $A_{bs} = 9.5 \times 10^{-5}$, $B_{bs} = -4.0 \times 10^{-5}$, $\tau = 1.1$, and $\delta = 10$. For given values of the branching ratios, the parameters g_X and $m_{Z'}$ are linearly dependent. This is because these two parameters always come in the term of $\frac{g_X^2}{m_{Z'}^2}$ in the expression of the Wilson coefficients when $k = 0$. For each constraints on R_K , R_{K^*} , $BR(B^+ \rightarrow K^+ \mu^+ \mu^-)$, and $BR(B^0 \rightarrow K^{*0} \mu^+ \mu^-)$, there are two separated range of the ratio $\frac{g_X^2}{m_{Z'}^2}$. However, there is only one overlapping region satisfying all of these four constraints. Furthermore, this allowed region is much more severe than the overlapping region determined by only two constraints from R_K and R_{K^*} (the blue hatched and the green regions). Therefore, additional consideration of the branching ratios of the decay processes $B^+ \rightarrow K^+ \mu^+ \mu^-$ and $B^0 \rightarrow K^{*0} \mu^+ \mu^-$ (the red hatched and the yellow regions) is crucial. The viable parameter region from all of these four constraints is plotted separately in Figure 17. From this, we can determine the allowed range for the ratio $\frac{g_X}{m_{Z'}}$ to be $0.0187\text{--}0.0216 \text{ GeV}^{-1}$. Taking into account the perturbation limit for g_X , we find the upper bound for $m_{Z'}$ to be approximately 190 GeV in this case.

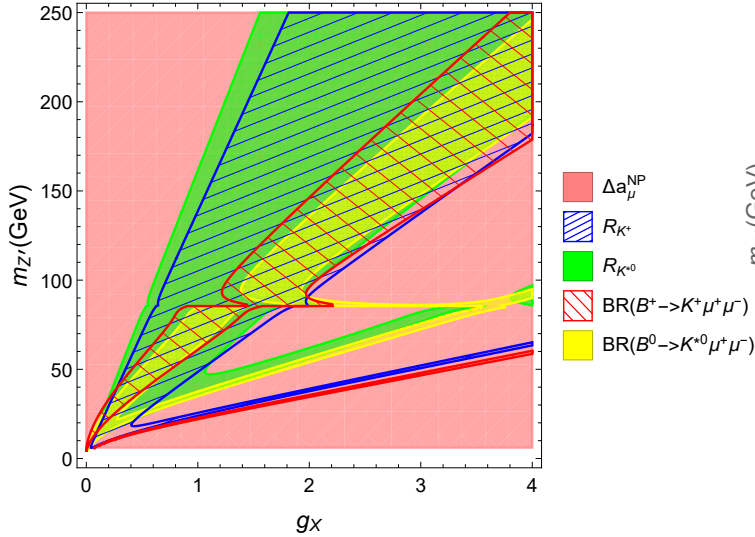


Figure 18: Phenomenological constraints on the $(g_X, m_{Z'})$ plane for the case of $y_\mu = 2$, $A_{bs} = 9.5 \times 10^{-5}$, $B_{bs} = -4.0 \times 10^{-5}$, $\tau = 1.1$, $\delta = 10$, and $k = 0.09$.

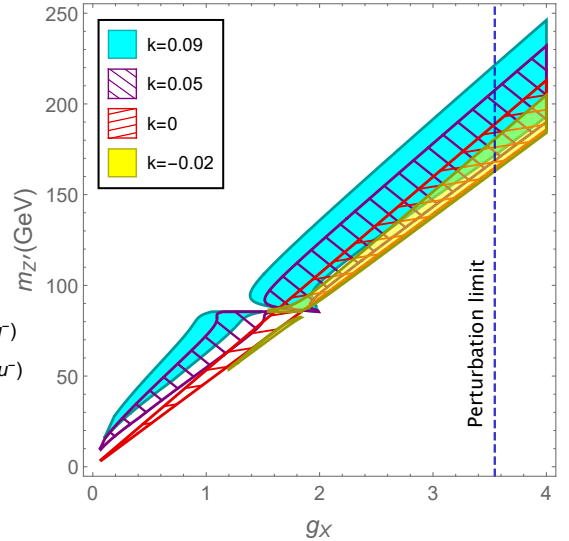


Figure 19: Viable parameter regions on the $(g_X, m_{Z'})$ plane for the case of $y_\mu = 2$, $A_{bs} = 9.5 \times 10^{-5}$, $B_{bs} = -4.0 \times 10^{-5}$, $\tau = 1.1$, $\delta = 10$, and various values of the kinetic mixing coefficient $k = -0.02, 0, 0.05, 0.09$.

When the gauge kinetic mixing is switched on, the linear correlation between g_X and $m_{Z'}$ is deformed due to nonzero values of k in the Wilson coefficients. In Figure 18, we demonstrate the phenomenological constraints on the $(g_X, m_{Z'})$ plane for $k = 0.09$. Here, the deformation

appears when $m_{Z'} \approx 85$ GeV is due to the sign flipping of the ZZ' mixing angle, α_Z , in Eq. (37). Furthermore, another effect of the gauge kinetic mixing is observed when the two separated regions corresponding to different values of the ratio $\frac{g_X}{m_{Z'}}$ for given values of the branching fractions (for example, the yellow regions corresponding to the constraint on $BR(B^0 \rightarrow K^{*0} \mu^+ \mu^-)$) in Figure 16 become connected for small values of g_X and $m_{Z'}$ in Figure 18. In the case with nonzero gauge kinetic mixing, the constraint from the muon $g - 2$ measurement need to be considered since Δa_μ^{NP} depends on $m_{Z'}$ via the β term in Eq. (54). For $k = 0.09$, we find the lower bound for the Z' -boson mass from this constraint to be $m_{Z'} \gtrsim 6.1$ GeV. In Figure 19, we plot the viable parameter regions for various values of the kinetic mixing coefficients, $k = -0.02, 0, 0.05$, and 0.09 . Comparing these areas, we see that, for larger values of k , the allowed region is larger, and the ratio $\frac{g_X}{m_{Z'}}$ tends to be smaller. The latter implies that larger values of $m_{Z'}$ are more favored for a given value of g_X . On the other hand, the perturbation limit for g_X is important in ruling out the region with large Z' -boson mass. Hence, it sets the upper limit for $m_{Z'}$ for fixed values of other parameters.

Constraints on the $(y_\mu, m_{Z'})$ plane:

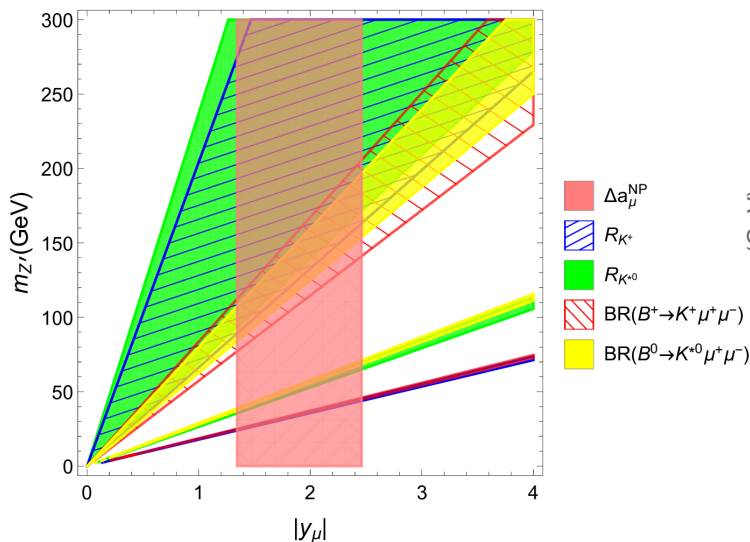


Figure 20: Phenomenological constraints on the $(y_\mu, m_{Z'})$ plane for the case of $m_{\chi_r} = 70$ GeV, $g_X = 3$, $A_{bs} = 9.5 \times 10^{-5}$, $B_{bs} = -4.0 \times 10^{-5}$, $\tau = 1.1$, $\delta = 10$, and $k = 0$.

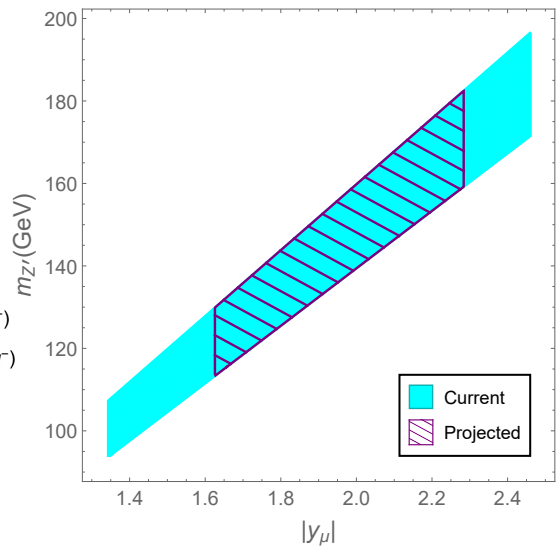


Figure 21: Viable parameter region on the $(y_\mu, m_{Z'})$ plane for the case of $m_{\chi_r} = 70$ GeV, $g_X = 3$, $A_{bs} = 9.5 \times 10^{-5}$, $B_{bs} = -4.0 \times 10^{-5}$, $\tau = 1.1$, $\delta = 10$, and $k = 0$.

The phenomenological constraints on the $(y_\mu, m_{Z'})$ plane are plotted in Figure 20 where the values of other fixed inputs are $m_{\chi_r} = 70$ GeV, $g_X = 3$, $A_{bs} = 9.5 \times 10^{-5}$, $B_{bs} = -4.0 \times 10^{-5}$, $\tau = 1.1$, $\delta = 10$, and $k = 0$, respectively. Since $m_{Z'}$ is not involved in the new physics contribution at the one-loop level to the muon $g - 2$ when $k = 0$, the constraint on Δa_μ^{NP} is a

vertical band in this figure. This constraint leads to the same limits for y_μ as those in Figure 12. Similar to Figure 16, the B -meson decay width leads to a linear dependence between these two parameters (y_μ and $m_{Z'}$) on the plane due to the factor $\frac{|y_\mu|}{m_{Z'}}$ in the Wilson coefficients when there is no kinetic mixing. In particular, each of the constraints on R_K , R_{K^*} , $BR(B^+ \rightarrow K^+ \mu^+ \mu^-)$, and $BR(B^0 \rightarrow K^{*0} \mu^+ \mu^-)$ determines two allowed ranges for the values of the ratio $\frac{|y_\mu|}{m_{Z'}}$. However, there is only one overlapping region with $0.0125 \text{ GeV}^{-1} \lesssim \frac{|y_\mu|}{m_{Z'}} \lesssim 0.0144 \text{ GeV}^{-1}$ that satisfies all of the considered 2σ bounds. This region is shown separately in Figure 21 with the cyan color. From this, we can extract the limits for the Z' -boson mass at 95% C.L. as $93.2 \text{ GeV}^{-1} \lesssim m_{Z'} \lesssim 197.3 \text{ GeV}^{-1}$. In the near future, when the E989 experiment get the results, assuming the center value of the muon $g - 2$ remains the same, we can expect the new limits for the Z' -boson mass to narrow down to $112.8 \text{ GeV}^{-1} \lesssim m_{Z'} \lesssim 182.9 \text{ GeV}^{-1}$ as illustrated by the hatched region.

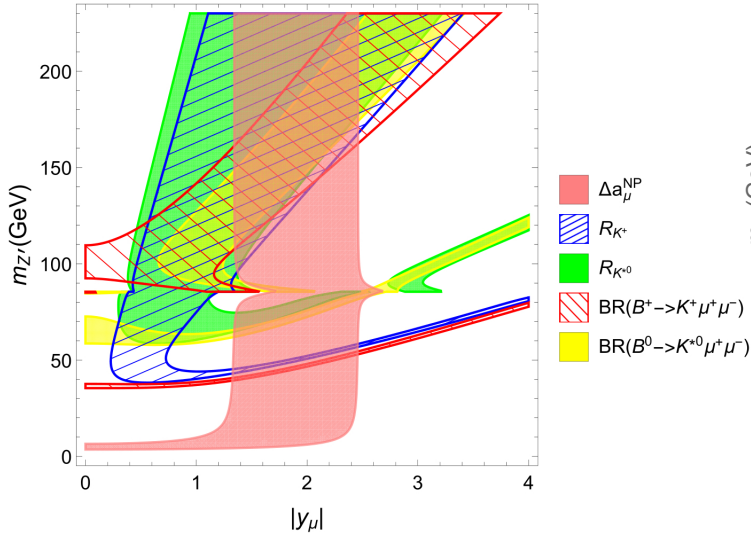


Figure 22: Phenomenological constraints on the $(y_\mu, m_{Z'})$ plane for the case of $m_{\chi_r} = 70 \text{ GeV}$, $g_X = 3$, $A_{bs} = 9.5 \times 10^{-5}$, $B_{bs} = -4.0 \times 10^{-5}$, $\tau = 1.1$, $\delta = 10$, and $k = 0.09$.

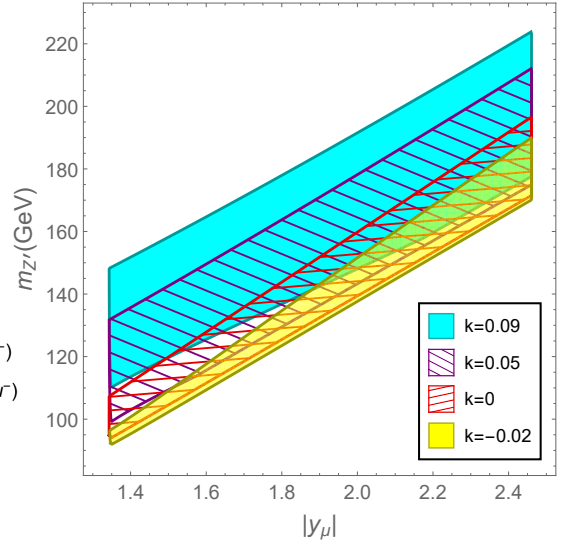


Figure 23: Viable parameter regions on the $(y_\mu, m_{Z'})$ plane for the case of $m_{\chi_r} = 70 \text{ GeV}$, $g_X = 3$, $A_{bs} = 9.5 \times 10^{-5}$, $B_{bs} = -4.0 \times 10^{-5}$, $\tau = 1.1$, $\delta = 10$, and various values of the kinetic mixing coefficient $k = -0.02, 0, 0.05, 0.09$.

When the gauge kinetic mixing is introduced, the constrained regions are strongly distorted as depicted in Figure 22 for the case of $k = 0.09$. On the one hand, regarding the constraint on Δa_μ^{NP} (the pink region), we see that the new Yukawa coupling, y_μ , can be small in the presence of the kinetic mixing term as the Z' boson is light enough with its mass of less than about 9 GeV. On the other hand, the constraint on the branching ratio of the decay process $B^+ \rightarrow K^+ \mu^+ \mu^-$

imply that $m_{Z'}$ must be larger than about 35 GeV. Therefore, small values of y_μ are forbidden in the case $k = 0.09$. The blue hatched region (the green region) determined by the bounds on R_K (R_{K^*}), which contains two separated ranges of the ratio $\frac{|y_\mu|}{m_{Z'}}$ as in Figure 20, become connected in this case. The red hatched and the yellow regions determined by the bounds on $BR(B^+ \rightarrow \mu^+ \mu^-)$ and $BR(B^0 \rightarrow \mu^+ \mu^-)$ also experience strong deformations particularly when $35 \text{ GeV} \lesssim m_{Z'} \lesssim 110 \text{ GeV}$. Especially, all the constrained regions are deformed when the Z' -boson mass is close to about 85 GeV where the mixing angle α_Z changes its sign. The viable parameter regions on the plane $(y_\mu, m_{Z'})$ satisfying all the considered constraints are presented in Figure 23 for different values of the gauge kinetic mixing coefficient $k = -0.02, 0, 0.05$, and 0.09 . We observe that the viable region shifts up when increasing the coefficient k . This indicates that larger values of $m_{Z'}$ are more favored for larger values of k as y_μ is fixed. Meanwhile, the allowed range for y_μ is almost independent on the gauge kinetic mixing coefficient k .

Constraints on k :

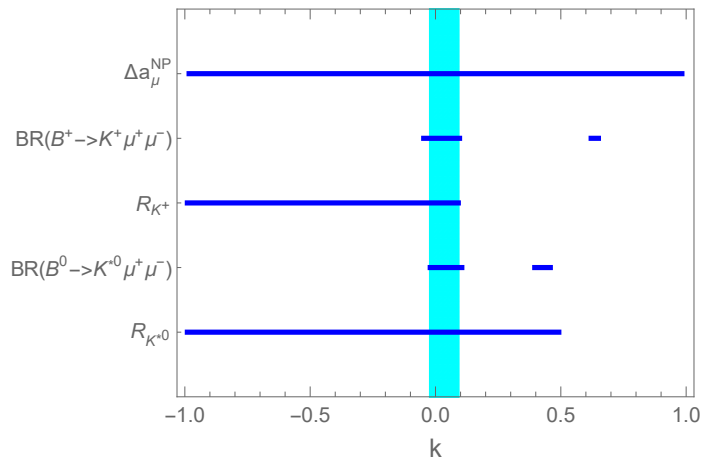


Figure 24: Phenomenological constraints on the gauge kinetic mixing coefficient for the case of $m_{\chi_r} = 70 \text{ GeV}$, $m_{Z'} = 150 \text{ GeV}$, $y_\mu = 2$, $g_X = 3$, $A_{bs} = 9.6 \times 10^{-5}$, $B_{bs} = -3.0 \times 10^{-5}$, $\tau = 1.1$, and $\delta = 10$.

The phenomenological constraints on the gauge kinetic mixing coefficient k are plotted in Figure 24 when other parameters are fixed as $m_{\chi_r} = 70 \text{ GeV}$, $m_{Z'} = 150 \text{ GeV}$, $y_\mu = 2$, $g_X = 3$, $A_{bs} = 9.6 \times 10^{-5}$, $B_{bs} = -3.0 \times 10^{-5}$, $\tau = 1.1$, and $\delta = 10$. We observe that the constraint on Δa_μ^{NP} only excludes large values of k being close to ± 1 . The R_K and R_{K^*} constraints are quite severe since they rule out large portions of the possible range of k . The most stringent limits on k are given by the constraints on the branching ratios of the decay processes $B^+ \rightarrow K^+ \mu^+ \mu^-$ and

$B^0 \rightarrow K^{*0} \mu^+ \mu^-$. There are two narrow ranges of k satisfying each of these two constraints. This observation once again reveals how important these branching ratios are beside R_K and R_{K^*} . By overlapping all the ranges of k allowed by the considered constraints, we find the viable range of the kinetic mixing coefficient to be $-0.021 \lesssim k \lesssim 0.091$ when other parameters are fixed. In Table 2, as a demonstration, the relevant observables are calculated for four benchmark values of the gauge kinetic mixing $k = -0.02, 0, 0.05$, and 0.09 while other parameters are chosen the same as those in Figure 24. All of them satisfy the corresponding experimental bounds at the 2σ level. We notice that, in this table, while the values of Δa_μ^{NP} only show the differences from the fifth significant digit when changing k , differences for the values of other observables can be seen from the second significant digit. It implies that the gauge kinetic mixing coefficient has a small effect on the muon $g - 2$, and sizable effects on the semileptonic B decays and the violation of lepton universality.

k	Δa_μ^{NP}	$\mathcal{B}(B^+ \rightarrow K^+ \mu^+ \mu^-)$	R_K	$\mathcal{B}(B^0 \rightarrow K^{*0}(892) \mu^+ \mu^-)$	R_{K^*}
-0.02	2.860396×10^{-9}	1.2740×10^{-7}	0.75503	1.9635×10^{-7}	0.60701
0	2.860402×10^{-9}	1.2333×10^{-7}	0.75170	1.8541×10^{-7}	0.59962
0.05	2.860370×10^{-9}	1.1357×10^{-7}	0.74252	1.6080×10^{-7}	0.58119
0.09	2.860299×10^{-9}	1.0613×10^{-7}	0.73423	1.4388×10^{-7}	0.56723

Table 2: The considered observables for the case of $m_{\chi_r} = 70$ GeV, $m_{Z'} = 150$ GeV, $y_\mu = 2$, $g_X = 3$, $A_{bs} = 9.6 \times 10^{-5}$, $B_{bs} = -3.0 \times 10^{-5}$, $\tau = 1.1$, $\delta = 10$, and four benchmark values of the gauge kinetic mixing coefficient k .

5 Conclusion

The BDW model with additional vector-like lepton and quark doublets and two complex scalars charged under the $U(1)_X$ gauge group is well motivated due to its ability in explaining various anomalies at the same time. In this paper, we have generalized this model by introducing the gauge kinetic mixing term. The new physics contributions to the muon anomalous magnetic moment and the Wilson coefficients ($C_{9,10}^{(\prime)}$) have been calculated analytically. We have investigated the parameter space of the model taking into account the phenomenological constraints to the muon $g - 2$, the updated LHCb data on lepton universality violation (R_K and R_{K^*}), and the branching ratios of the semileptonic rare decays ($B^+ \rightarrow K^+ \mu^+ \mu^-$ and $B^0 \rightarrow K^0 \mu^+ \mu^-$), as well as requirements from the perturbative theory. The viable parameter regions satisfying all the considered constraints at the level of 2σ have been identified. The results indicate that the FCNC parameters, A_{bs} and B_{bs} , must be as small as $\mathcal{O}(10^{-4}-10^{-5})$ to be consistent with experiment data. In the presence of the gauge kinetic mixing term, the allowed regions are

shifted and significantly deformed in comparison to the case with $k = 0$. Especially, the kinetic mixing coefficient plays an important role in extending the viable parameter regions. In the near future, with the projected sensitivity, the E989 experiment will be able to test certain parts of the free parameter space and put a more severe constraint on the acceptable parameter regions of the model.

Acknowledgment

We would like to thank Prof. Nguyen Xuan Han for his enthusiasm and encouragement on this work.

References

- [1] M. Tanabashi *et al.* [Particle Data Group], Phys. Rev. D **98**, no.3, 030001 (2018); P. J. Mohr, B. N. Taylor and D. B. Newell, Rev. Mod. Phys. **84**, 1527-1605 (2012) [arXiv:1203.5425 [physics.atom-ph]]; G. W. Bennett *et al.* [Muon g-2], Phys. Rev. Lett. **89**, 101804 (2002) [arXiv:hep-ex/0208001 [hep-ex]]; G. W. Bennett *et al.* [Muon g-2], Phys. Rev. Lett. **89**, 101804 (2002) [arXiv:hep-ex/0208001 [hep-ex]]; G. W. Bennett *et al.* [Muon g-2], Phys. Rev. Lett. **92**, 161802 (2004) [arXiv:hep-ex/0401008 [hep-ex]]; G. W. Bennett *et al.* [Muon g-2], Phys. Rev. D **73**, 072003 (2006) [arXiv:hep-ex/0602035 [hep-ex]].
- [2] T. Aoyama *et al.*, [arXiv:2006.04822 [hep-ph]]; T. Aoyama, M. Hayakawa, T. Kinoshita and M. Nio, Phys. Rev. Lett. **109**, 111808 (2012) [arXiv:1205.5370 [hep-ph]]; T. Aoyama, T. Kinoshita and M. Nio, Phys. Rev. D **97**, no.3, 036001 (2018) [arXiv:1712.06060 [hep-ph]]; C. Gnendiger, D. Stöckinger and H. Stöckinger-Kim, Phys. Rev. D **88**, 053005 (2013) [arXiv:1306.5546 [hep-ph]]; T. Blum, A. Denig, I. Logashenko, E. de Rafael, B. L. Roberts, T. Teubner and G. Venanzoni, [arXiv:1311.2198 [hep-ph]]; M. Davier, A. Hoecker, B. Malaescu and Z. Zhang, Eur. Phys. J. C **71**, 1515 (2011) [arXiv:1010.4180 [hep-ph]]; M. Davier, A. Hoecker, B. Malaescu and Z. Zhang, Eur. Phys. J. C **77**, no.12, 827 (2017) [arXiv:1706.09436 [hep-ph]]; M. Davier, A. Hoecker, B. Malaescu and Z. Zhang, Eur. Phys. J. C **80**, no.3, 241 (2020) [arXiv:1908.00921 [hep-ph]]. For early analyses of the muon $g - 2$, see for example, H. Terazawa, Prog. Theor. Phys. **39**, 1326-1332 (1968); H. Terazawa, Phys. Rev. **177**, 2159-2166 (1969); H. Terazawa, Prog. Theor. Phys. **40**, 830-833 (1968).
- [3] J. Grange *et al.* [Muon g-2], [arXiv:1501.06858 [physics.ins-det]]; A. T. Fienberg [Muon g-2], [arXiv:1905.05318 [hep-ex]].

- [4] T. Mibe [J-PARC g-2], Chin. Phys. C **34**, 745-748 (2010)
- [5] A. Keshavarzi, D. Nomura and T. Teubner, Phys. Rev. D **97**, no.11, 114025 (2018) [arXiv:1802.02995 [hep-ph]].
- [6] See for example, H. M. Tran and H. T. Nguyen, Phys. Rev. D **99** (2019) no.3, 035040 [arXiv:1812.11757 [hep-ph]].
- [7] R. Aaij *et al.* [LHCb], Phys. Rev. Lett. **122**, no.19, 191801 (2019) [arXiv:1903.09252 [hep-ex]]; R. Aaij *et al.* [LHCb], Phys. Rev. Lett. **113**, 151601 (2014) [arXiv:1406.6482 [hep-ex]].
- [8] R. Aaij *et al.* [LHCb], JHEP **08**, 055 (2017) [arXiv:1705.05802 [hep-ex]]; A. Abdesselam *et al.* [Belle], [arXiv:1904.02440 [hep-ex]].
- [9] C. Bouchard *et al.* [HPQCD], Phys. Rev. Lett. **111**, no.16, 162002 (2013) [arXiv:1306.0434 [hep-ph]].
- [10] C. Bobeth, G. Hiller and G. Piranishvili, JHEP **12**, 040 (2007) [arXiv:0709.4174 [hep-ph]].
- [11] G. Hiller and F. Kruger, Phys. Rev. D **69**, 074020 (2004) [arXiv:hep-ph/0310219 [hep-ph]].
- [12] M. Bordone, G. Isidori and A. Pattori, Eur. Phys. J. C **76**, no.8, 440 (2016) [arXiv:1605.07633 [hep-ph]].
- [13] A. K. Alok, A. Dighe, S. Gangal and D. Kumar, JHEP **06**, 089 (2019) [arXiv:1903.09617 [hep-ph]].
- [14] R. Aaij *et al.* [LHCb], Phys. Rev. Lett. **125**, no.1, 011802 (2020) [arXiv:2003.04831 [hep-ex]].
- [15] S. Descotes-Genon, T. Hurth, J. Matias and J. Virto, JHEP **05**, 137 (2013) [arXiv:1303.5794 [hep-ph]].
- [16] R. Aaij *et al.* [LHCb], JHEP **02**, 104 (2016) [arXiv:1512.04442 [hep-ex]].
- [17] B. Grinstein, M. J. Savage and M. B. Wise, Nucl. Phys. B **319**, 271-290 (1989); G. Buchalla, A. J. Buras and M. E. Lautenbacher, Rev. Mod. Phys. **68**, 1125-1144 (1996) [arXiv:hep-ph/9512380 [hep-ph]]; K. G. Chetyrkin, M. Misiak and M. Munz, Phys. Lett. B **400**, 206-219 (1997) [arXiv:hep-ph/9612313 [hep-ph]]; W. Altmannshofer, P. Ball, A. Bharucha, A. J. Buras, D. M. Straub and M. Wick, JHEP **01**, 019 (2009) [arXiv:0811.1214 [hep-ph]].

- [18] M. Algueró, B. Capdevila, A. Crivellin, S. Descotes-Genon, P. Masjuan, J. Matias, M. Novoa Brunet and J. Virto, *Eur. Phys. J. C* **79**, no.8, 714 (2019) [arXiv:1903.09578 [hep-ph]]; A. K. Alok, A. Dighe, S. Gangal and D. Kumar, *JHEP* **06**, 089 (2019) [arXiv:1903.09617 [hep-ph]]; M. Ciuchini, A. M. Coutinho, M. Fedele, E. Franco, A. Paul, L. Silvestrini and M. Valli, *Eur. Phys. J. C* **79**, no.8, 719 (2019) [arXiv:1903.09632 [hep-ph]]; G. D’Amico, M. Nardecchia, P. Panci, F. Sannino, A. Strumia, R. Torre and A. Urbano, *JHEP* **09**, 010 (2017) [arXiv:1704.05438 [hep-ph]]; A. Datta, J. Kumar and D. London, *Phys. Lett. B* **797**, 134858 (2019) [arXiv:1903.10086 [hep-ph]]; J. Aebischer, W. Altmannshofer, D. Guadagnoli, M. Reboud, P. Stangl and D. M. Straub, *Eur. Phys. J. C* **80**, no.3, 252 (2020) [arXiv:1903.10434 [hep-ph]]; A. Arbey, T. Hurth, F. Mahmoudi, D. M. Santos and S. Neshatpour, *Phys. Rev. D* **100** (2019) no.1, 015045 [arXiv:1904.08399 [hep-ph]].
- [19] R. Alonso, B. Grinstein and J. Martin Camalich, *Phys. Rev. Lett.* **113**, 241802 (2014) [arXiv:1407.7044 [hep-ph]]; W. Altmannshofer, C. Niehoff and D. M. Straub, *JHEP* **05**, 076 (2017) [arXiv:1702.05498 [hep-ph]].
- [20] A. Paul and D. M. Straub, *JHEP* **04**, 027 (2017) [arXiv:1608.02556 [hep-ph]].
- [21] K. Kowalska, D. Kumar and E. M. Sessolo, *Eur. Phys. J. C* **79** (2019) no.10, 840 [arXiv:1903.10932 [hep-ph]]. A. Vicente, [arXiv:2001.04788 [hep-ph]].
- [22] A. K. Alok, B. Bhattacharya, A. Datta, D. Kumar, J. Kumar and D. London, *Phys. Rev. D* **96**, no.9, 095009 (2017) [arXiv:1704.07397 [hep-ph]].
- [23] A. Biswas, S. Nandi, I. Ray and S. K. Patra, [arXiv:2004.14687 [hep-ph]].
- [24] D. Aristizabal Sierra, F. Staub and A. Vicente, *Phys. Rev. D* **92**, no.1, 015001 (2015) [arXiv:1503.06077 [hep-ph]]; S. Descotes-Genon, J. Matias and J. Virto, *Phys. Rev. D* **88**, 074002 (2013) [arXiv:1307.5683 [hep-ph]]; R. Gauld, F. Goertz and U. Haisch, *Phys. Rev. D* **89**, 015005 (2014) [arXiv:1308.1959 [hep-ph]]; W. Altmannshofer, S. Gori, M. Pospelov and I. Yavin, *Phys. Rev. D* **89**, 095033 (2014) [arXiv:1403.1269 [hep-ph]]; S. M. Boucenna, A. Celis, J. Fuentes-Martin, A. Vicente and J. Virto, *Phys. Lett. B* **760**, 214-219 (2016) [arXiv:1604.03088 [hep-ph]]; S. M. Boucenna, A. Celis, J. Fuentes-Martin, A. Vicente and J. Virto, *JHEP* **12**, 059 (2016) [arXiv:1608.01349 [hep-ph]]; E. Megias, M. Quiros and L. Salas, *JHEP* **05**, 016 (2017) [arXiv:1701.05072 [hep-ph]]; E. Megias, M. Quiros and L. Salas, *JHEP* **07**, 102 (2017) [arXiv:1703.06019 [hep-ph]]; E. Megias, M. Quiros and L. Salas, *Phys. Rev. D* **96**, no.7, 075030 (2017) [arXiv:1707.08014 [hep-ph]]; D. Borah, L. Mukherjee and S. Nandi, [arXiv:2007.13778 [hep-ph]].

- [25] A. J. Buras, F. De Fazio and J. Girrbach, *JHEP* **02**, 112 (2014) [arXiv:1311.6729 [hep-ph]]; A. J. Buras and J. Girrbach, *JHEP* **12**, 009 (2013) [arXiv:1309.2466 [hep-ph]]; A. Crivellin, G. D'Ambrosio and J. Heeck, *Phys. Rev. D* **91**, no.7, 075006 (2015) [arXiv:1503.03477 [hep-ph]]; A. Crivellin, G. D'Ambrosio and J. Heeck, *Phys. Rev. Lett.* **114**, 151801 (2015) [arXiv:1501.00993 [hep-ph]]; A. Celis, J. Fuentes-Martin, M. Jung and H. Serodio, *Phys. Rev. D* **92**, no.1, 015007 (2015) [arXiv:1505.03079 [hep-ph]]; A. Celis, W. Z. Feng and D. Lüster, *JHEP* **02**, 007 (2016) [arXiv:1512.02218 [hep-ph]]; A. Falkowski, M. Nardecchia and R. Ziegler, *JHEP* **11**, 173 (2015) [arXiv:1509.01249 [hep-ph]]; B. Allanach, F. S. Queiroz, A. Strumia and S. Sun, *Phys. Rev. D* **93**, no.5, 055045 (2016) [arXiv:1511.07447 [hep-ph]]; C. W. Chiang, X. G. He and G. Valencia, *Phys. Rev. D* **93**, no.7, 074003 (2016) [arXiv:1601.07328 [hep-ph]]; C. S. Kim, X. B. Yuan and Y. J. Zheng, *Phys. Rev. D* **93**, no.9, 095009 (2016) [arXiv:1602.08107 [hep-ph]]; P. Rocha-Moran and A. Vicente, *Phys. Rev. D* **99**, no.3, 035016 (2019) [arXiv:1810.02135 [hep-ph]].
- [26] S. Dwivedi, D. Kumar Ghosh, A. Falkowski and N. Ghosh, *Eur. Phys. J. C* **80**, no.3, 263 (2020) [arXiv:1908.03031 [hep-ph]]; B. C. Allanach and J. Davighi, *Eur. Phys. J. C* **79**, no.11, 908 (2019) [arXiv:1905.10327 [hep-ph]]; A. Biswas and A. Shaw, *JHEP* **05**, 165 (2019) [arXiv:1903.08745 [hep-ph]]; B. C. Allanach and J. Davighi, *JHEP* **12**, 075 (2018) [arXiv:1809.01158 [hep-ph]]; A. Falkowski, S. F. King, E. Perdomo and M. Pierre, *JHEP* **08**, 061 (2018) [arXiv:1803.04430 [hep-ph]]; R. Martinez, F. Ochoa and J. M. Quimbayo, *Phys. Rev. D* **98**, no.3, 035036 (2018) [arXiv:1712.06189 [hep-ph]]; S. F. King, *JHEP* **08**, 019 (2017) [arXiv:1706.06100 [hep-ph]]; J. M. Cline and J. Martin Camalich, *Phys. Rev. D* **96**, no.5, 055036 (2017) [arXiv:1706.08510 [hep-ph]]; C. W. Chiang, X. G. He, J. Tandean and X. B. Yuan, *Phys. Rev. D* **96**, no.11, 115022 (2017) [arXiv:1706.02696 [hep-ph]]; C. Bonilla, T. Modak, R. Srivastava and J. W. F. Valle, *Phys. Rev. D* **98**, no.9, 095002 (2018) [arXiv:1705.00915 [hep-ph]]; A. Celis, W. Z. Feng and M. Vollmann, *Phys. Rev. D* **95**, no.3, 035018 (2017) [arXiv:1608.03894 [hep-ph]]; L. Di Luzio, M. Kirk, A. Lenz and T. Rauh, *JHEP* **12**, 009 (2019) [arXiv:1909.11087 [hep-ph]]; A. Crivellin, L. Hofer, J. Matias, U. Nierste, S. Pokorski and J. Rosiek, *Phys. Rev. D* **92**, no.5, 054013 (2015) [arXiv:1504.07928 [hep-ph]].
- [27] G. Hiller and M. Schmaltz, *Phys. Rev. D* **90**, 054014 (2014) [arXiv:1408.1627 [hep-ph]]; S. Biswas, D. Chowdhury, S. Han and S. J. Lee, *JHEP* **02**, 142 (2015) [arXiv:1409.0882 [hep-ph]]; B. Gripaios, M. Nardecchia and S. A. Renner, *JHEP* **05**, 006 (2015) [arXiv:1412.1791 [hep-ph]]; I. Doršner, S. Fajfer, A. Greljo, J. F. Kamenik and N. Košnik, *Phys. Rept.* **641**, 1-68 (2016) [arXiv:1603.04993 [hep-ph]]; S. Saad and A. Thapa, *Phys. Rev. D* **102**, no.1, 015014 (2020) [arXiv:2004.07880 [hep-ph]].

- [28] B. Gripaios, M. Nardecchia and S. A. Renner, JHEP **06**, 083 (2016) [arXiv:1509.05020 [hep-ph]]; P. Arnan, L. Hofer, F. Mescia and A. Crivellin, JHEP **04**, 043 (2017) [arXiv:1608.07832 [hep-ph]].
- [29] W. Altmannshofer, P. S. B. Dev, A. Soni and Y. Sui, [arXiv:2002.12910 [hep-ph]]; S. Khalil, J. Phys. G **45**, no.12, 125004 (2018) [arXiv:1706.07337 [hep-ph]].
- [30] G. Bélanger, C. Delaunay and S. Westhoff, Phys. Rev. D **92** (2015), 055021 [arXiv:1507.06660 [hep-ph]].
- [31] Y. S. Amhis *et al.* [HFLAV], [arXiv:1909.12524 [hep-ex]].
- [32] B. Holdom, Phys. Lett. B **166**, 196-198 (1986); P. H. Chankowski, S. Pokorski and J. Wagner, Eur. Phys. J. C **47**, 187-205 (2006) [arXiv:hep-ph/0601097 [hep-ph]]; B. Brahmachari and A. Raychaudhuri, Nucl. Phys. B **887**, 441-455 (2014) [arXiv:1409.2082 [hep-ph]]; K. S. Babu, C. F. Kolda and J. March-Russell, Phys. Rev. D **57**, 6788-6792 (1998) [arXiv:hep-ph/9710441 [hep-ph]].
- [33] F. del Aguila, G. D. Coughlan and M. Quiros, Nucl. Phys. B **307**, 633 (1988); Nucl. Phys. B **312**, 751 (1989) (erratum); F. del Aguila, J. A. Gonzalez and M. Quiros, Nucl. Phys. B **307**, 571-632 (1988).
- [34] R. M. Fonseca, M. Malinsky, W. Porod and F. Staub, Nucl. Phys. B **854**, 28-53 (2012) [arXiv:1107.2670 [hep-ph]]; B. O’Leary, W. Porod and F. Staub, JHEP **05**, 042 (2012) [arXiv:1112.4600 [hep-ph]]; L. Basso, B. O’Leary, W. Porod and F. Staub, JHEP **09**, 054 (2012) [arXiv:1207.0507 [hep-ph]]; J. Kalinowski, S. F. King and J. P. Roberts, JHEP **01**, 066 (2009) [arXiv:0811.2204 [hep-ph]]; G. Bélanger, J. Da Silva and H. M. Tran, Phys. Rev. D **95**, no.11, 115017 (2017) [arXiv:1703.03275 [hep-ph]].
- [35] Heavy Flavor Averaging Group, https://hflav-eos.web.cern.ch/hflav-eos/rare/April2019/RADLL/OUTPUT/HTML/radll_table1.html
- [36] R. Aaij *et al.* [LHCb], JHEP **02**, 105 (2013) [arXiv:1209.4284 [hep-ex]]; R. Aaij *et al.* [LHCb], JHEP **06**, 133 (2014) [arXiv:1403.8044 [hep-ex]].
- [37] R. Aaij *et al.* [LHCb], JHEP **11**, 047 (2016) [arXiv:1606.04731 [hep-ex]].
- [38] Heavy Flavor Averaging Group, https://hflav-eos.web.cern.ch/hflav-eos/rare/April2019/RADLL/OUTPUT/HTML/radll_table5.html
- [39] W. Altmannshofer and D. M. Straub, JHEP **08**, 121 (2012) [arXiv:1206.0273 [hep-ph]].

- [40] W. Wang and S. Zhao, Chin. Phys. C **42**, no.1, 013105 (2018) [arXiv:1704.08168 [hep-ph]].
- [41] C. Bobeth, G. Hiller and G. Piranishvili, JHEP **07**, 106 (2008) [arXiv:0805.2525 [hep-ph]].
- [42] A. Bharucha, T. Feldmann and M. Wick, JHEP **09**, 090 (2010) [arXiv:1004.3249 [hep-ph]].